From the Micro to the Macro:

Bridging the Gap Between The Theory and Observation of Blazar Jets

Nicholas MacDonald
Max Planck Institute for Radio Astronomy

Half a Century of Blazars and Beyond

Torino, Italy
June 14th 2018

Talk Outline

Synthetic Single Dish TEMZ Model Light Curves

Synthetic GMVA Imaging of the TEMZ Model

Ray-tracing Through a Relativistic PIC Jet Simulation

Ray-tracing Through an RMHD Jet Simulation

Stacked Rotation Measure Mapping

Half a Century of Blazars and Beyond

Torino, Italy
June 14th 2018

Synthetic Single Dish TEMZ Model Light Curves

POLAMI Program

POLAMI

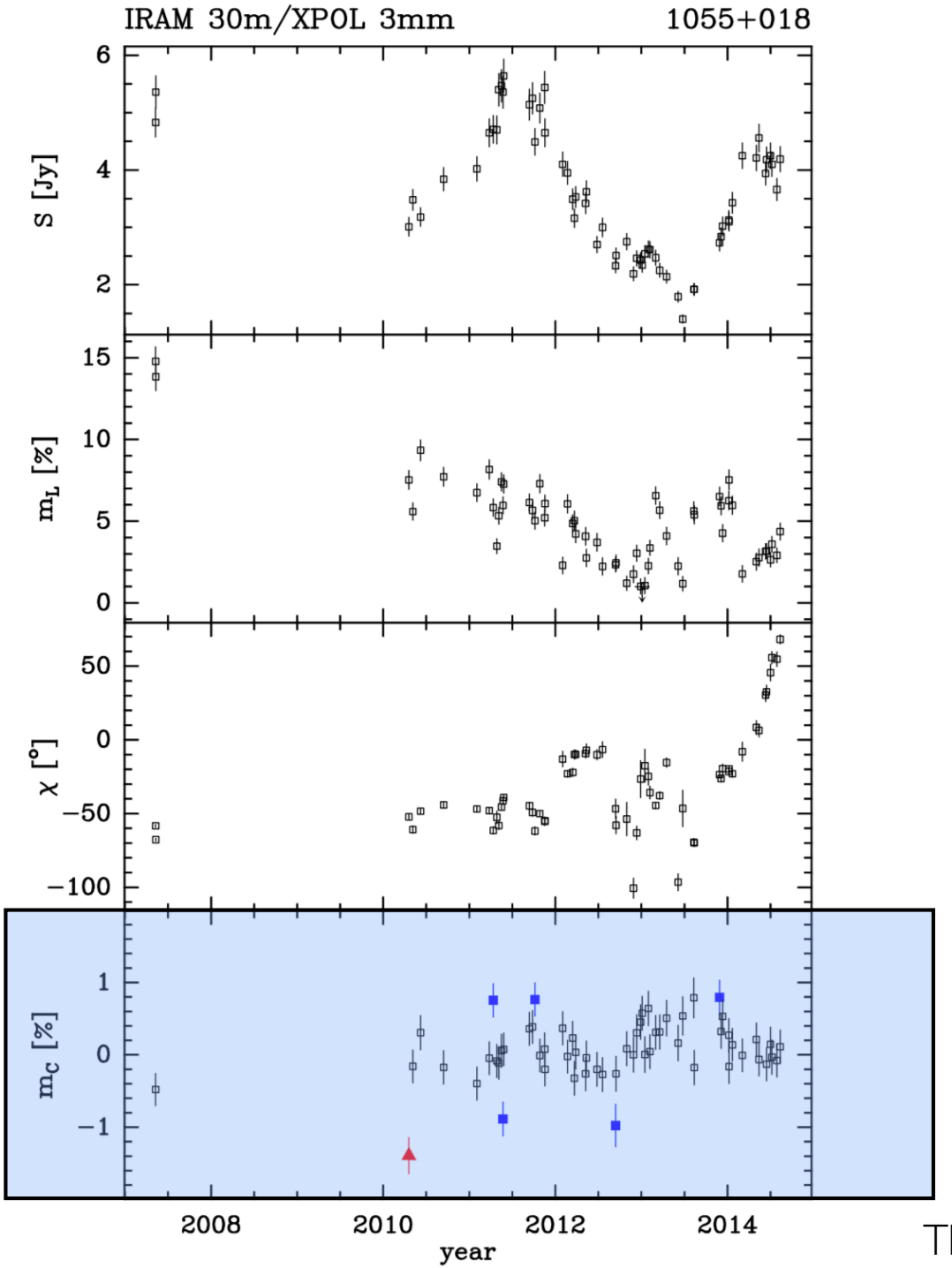

Thum et al. (2018)


Recollimation Shock

The Turbulent Extreme Multi-Zone (TEMZ) Model

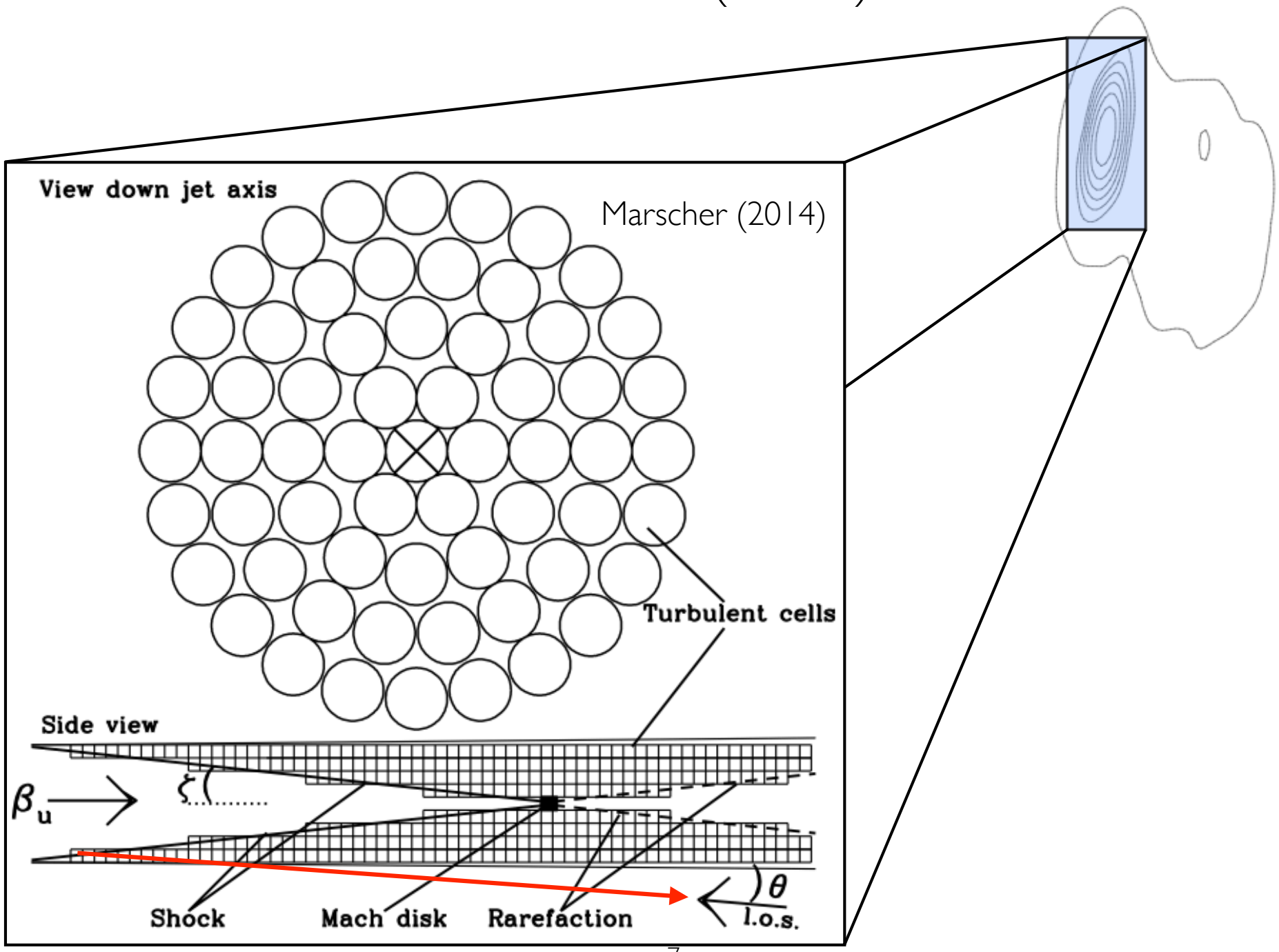

The Full Stokes Equations of Polarized Radiative Transfer:

$$\begin{Bmatrix} \left(\frac{d}{dl}+\kappa_I\right) & \kappa_Q & \kappa_U & \kappa_V \\ \kappa_Q & \left(\frac{d}{dl}+\kappa_I\right) & \kappa^*{}_V & -\kappa^*{}_U \\ \kappa_U & -\kappa^*{}_V & \left(\frac{d}{dl}+\kappa_I\right) & \kappa^*{}_Q \\ \kappa_V & \kappa^*{}_U & -\kappa^*{}_Q & \left(\frac{d}{dl}+\kappa_I\right) \end{Bmatrix} \begin{Bmatrix} I_\nu \\ Q_\nu \\ U_\nu \\ V_\nu \end{Bmatrix} = \begin{Bmatrix} \eta_\nu{}^I \\ \eta_\nu{}^Q \\ \eta_\nu{}^U \\ \eta_\nu{}^V \end{Bmatrix}$$

Jones & O'Dell (1977)

The RADMC-3D Code

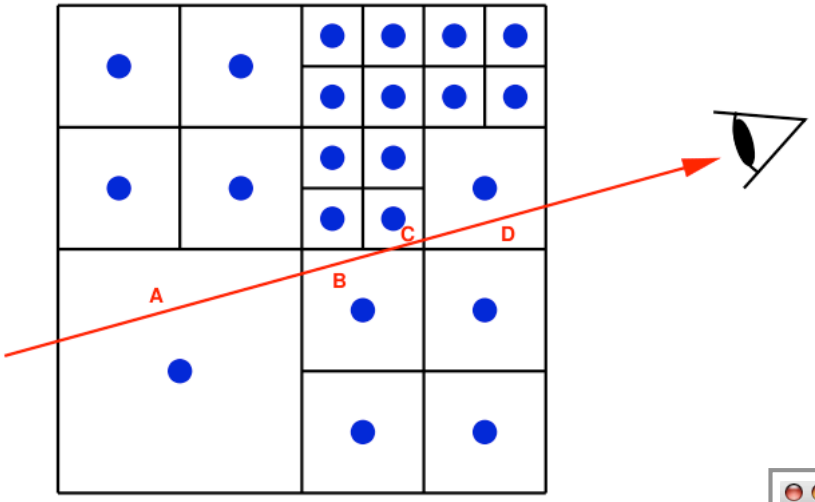

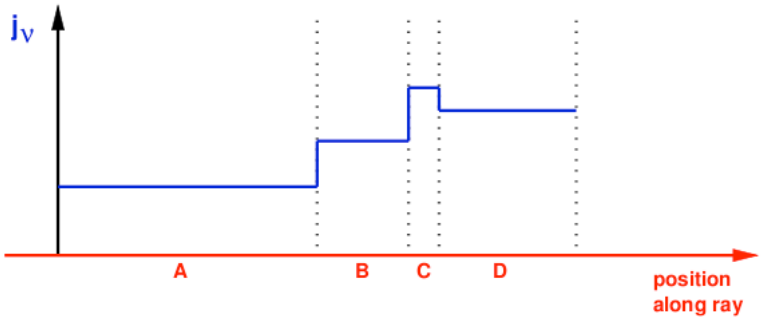

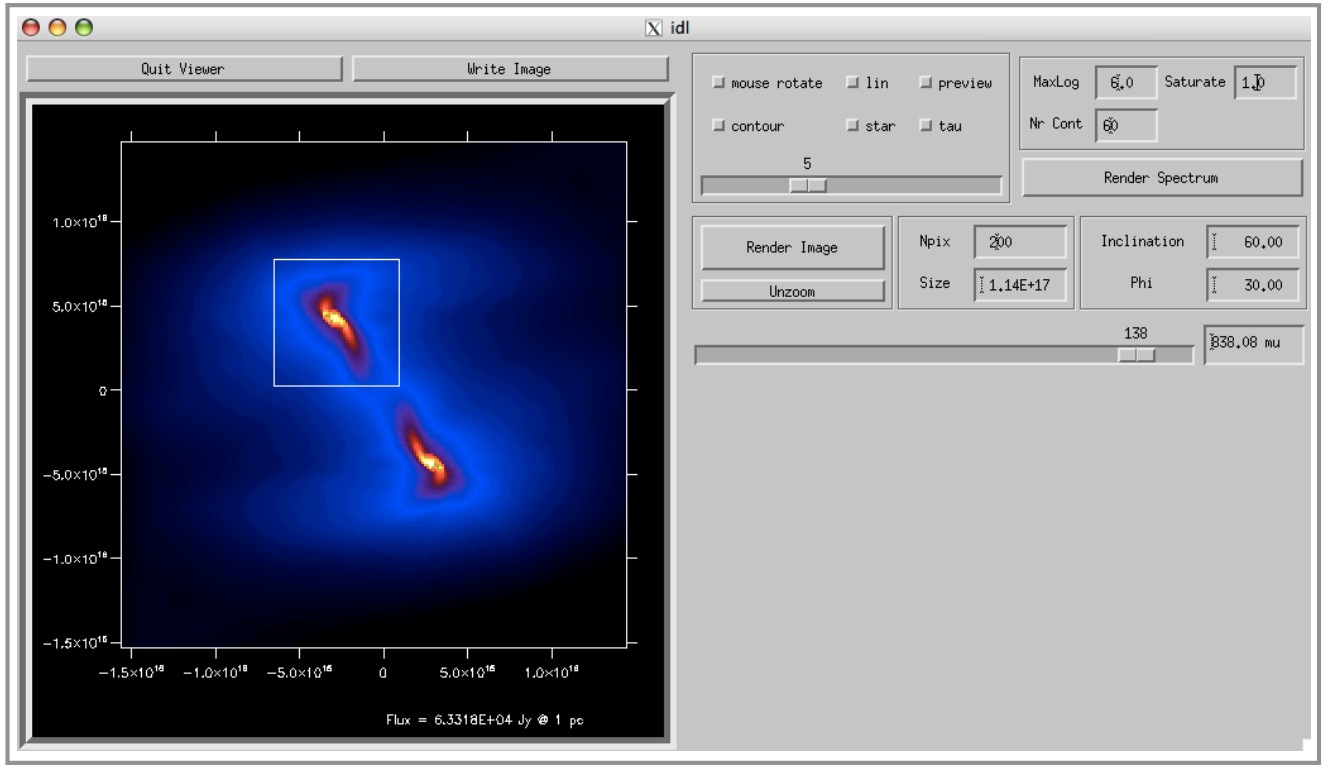

Dullemond (2015)

TEMZ Modeling

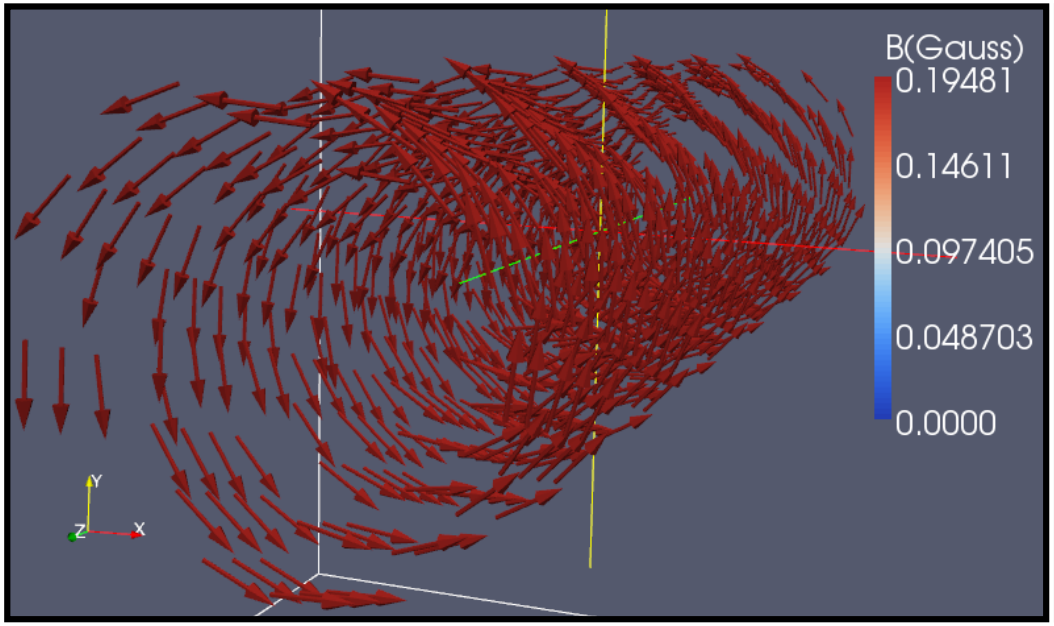

Helical Jet

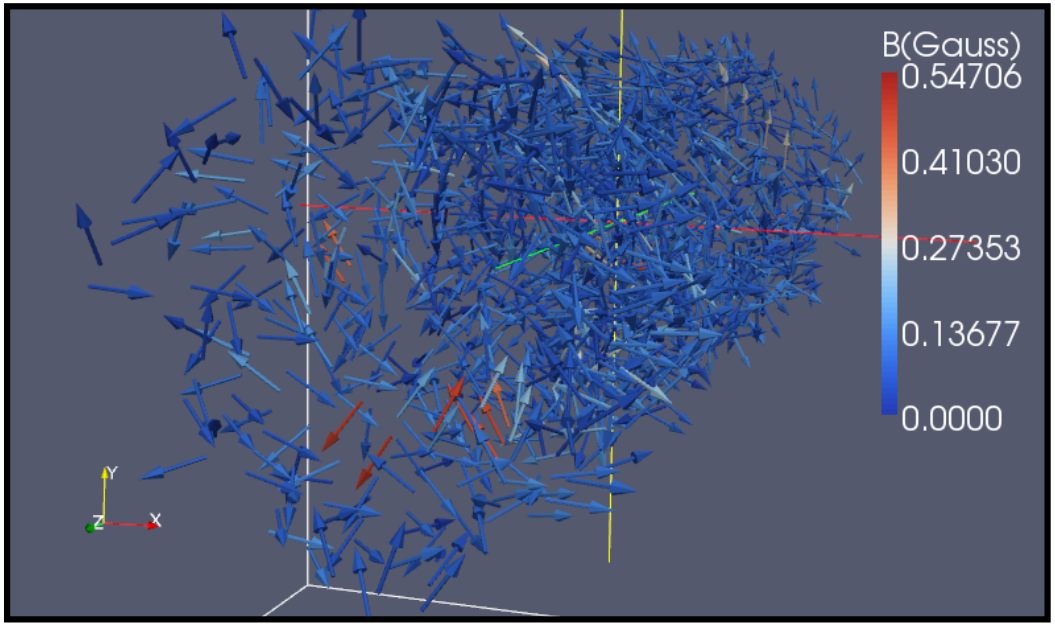

Turbulent Jet

MacDonald & Marscher (in press)

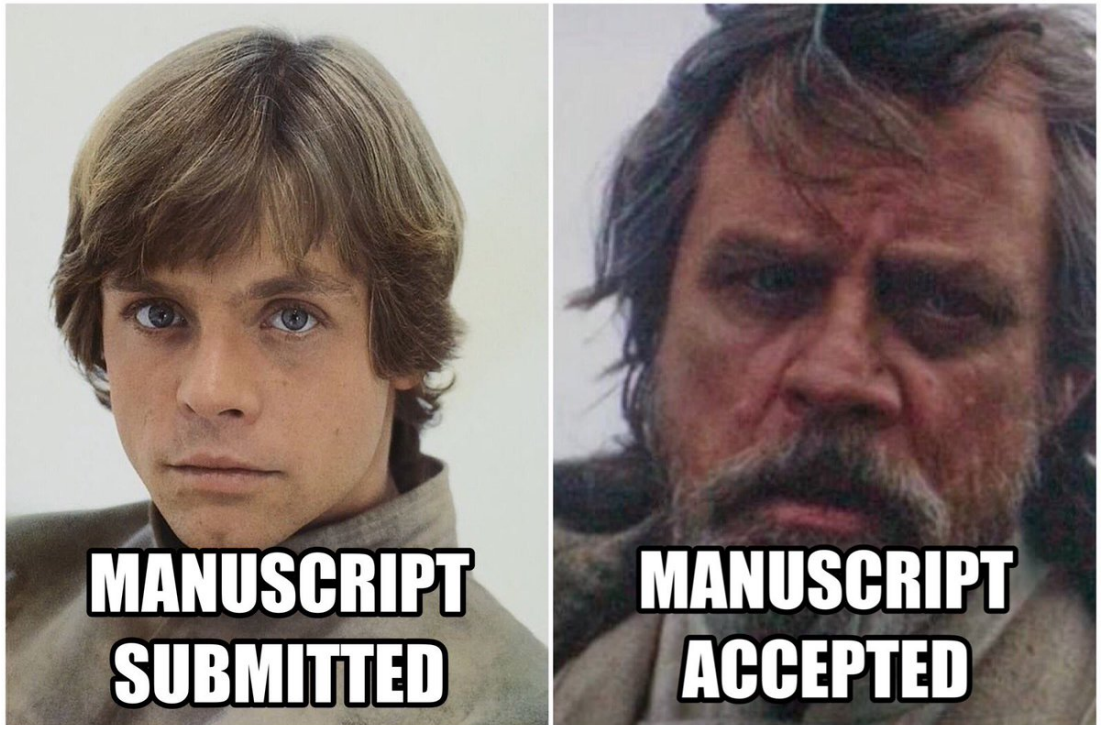
MANUSCRIPT
SUBMITTED
MANUSCRIPT
ACCEPTED

TEMZ Imaging

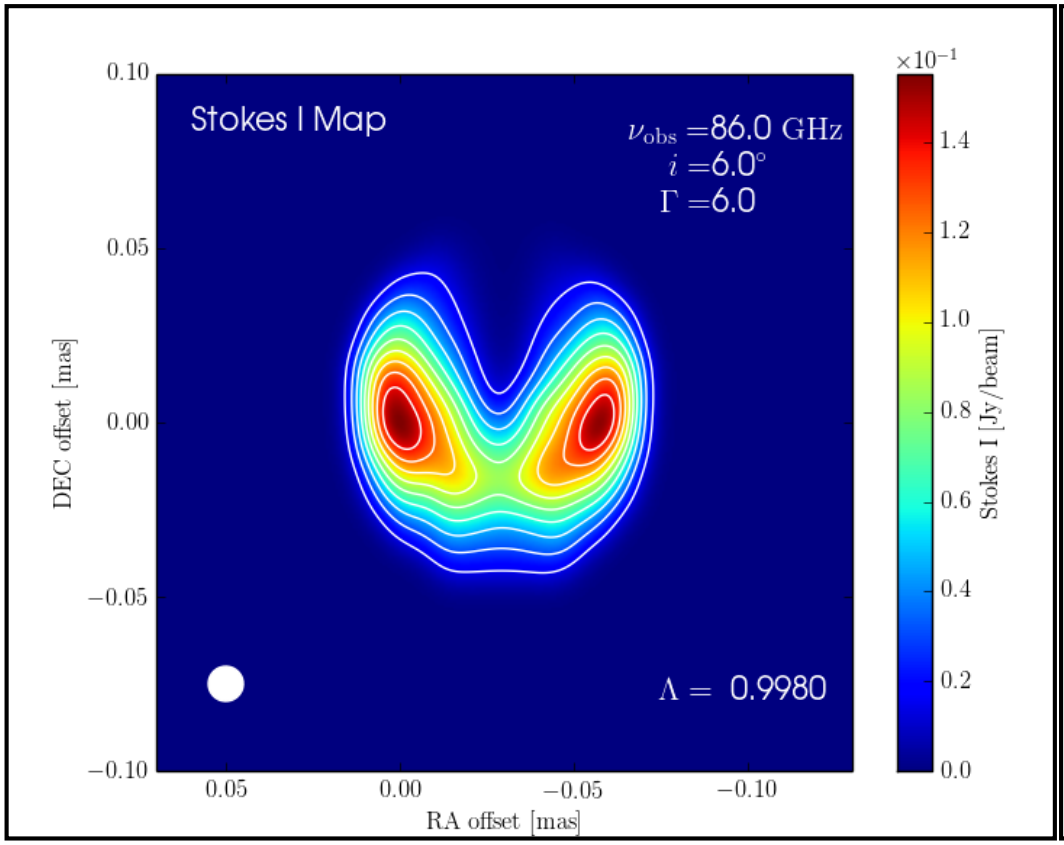

Helical Jet

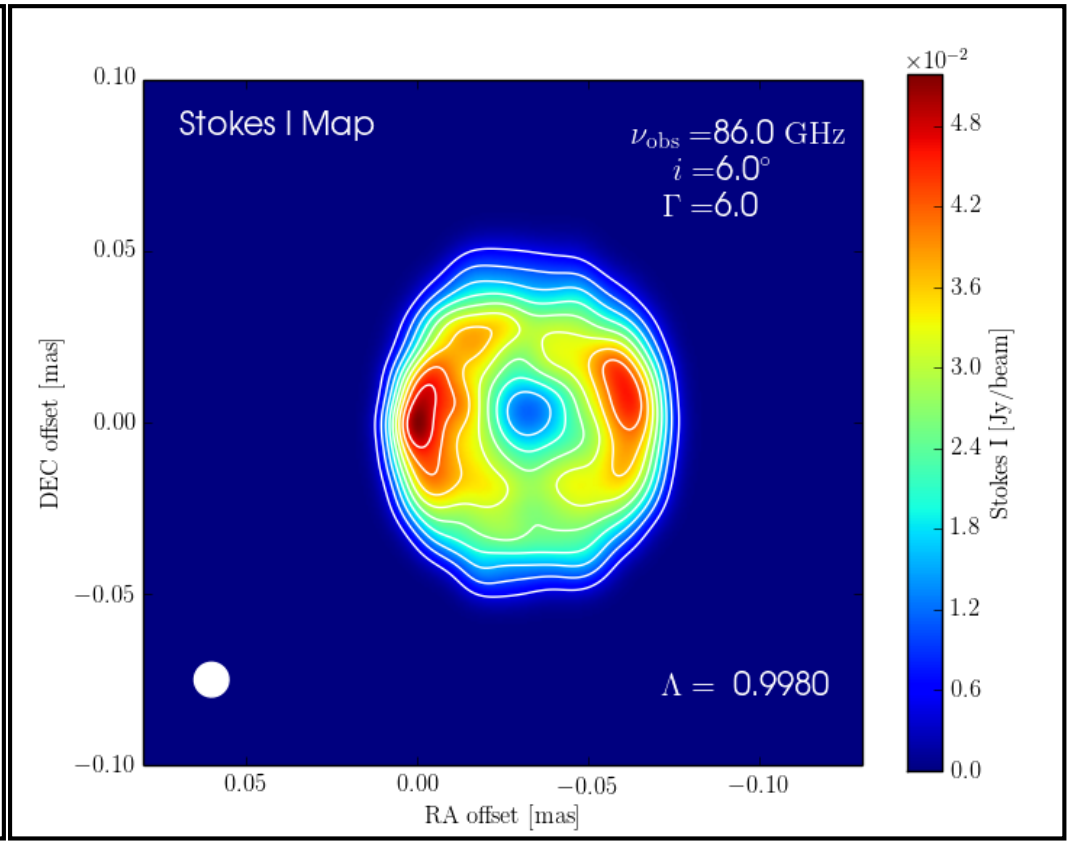

Turbulent Jet

MacDonald & Marscher (in press)

TEMZ Imaging

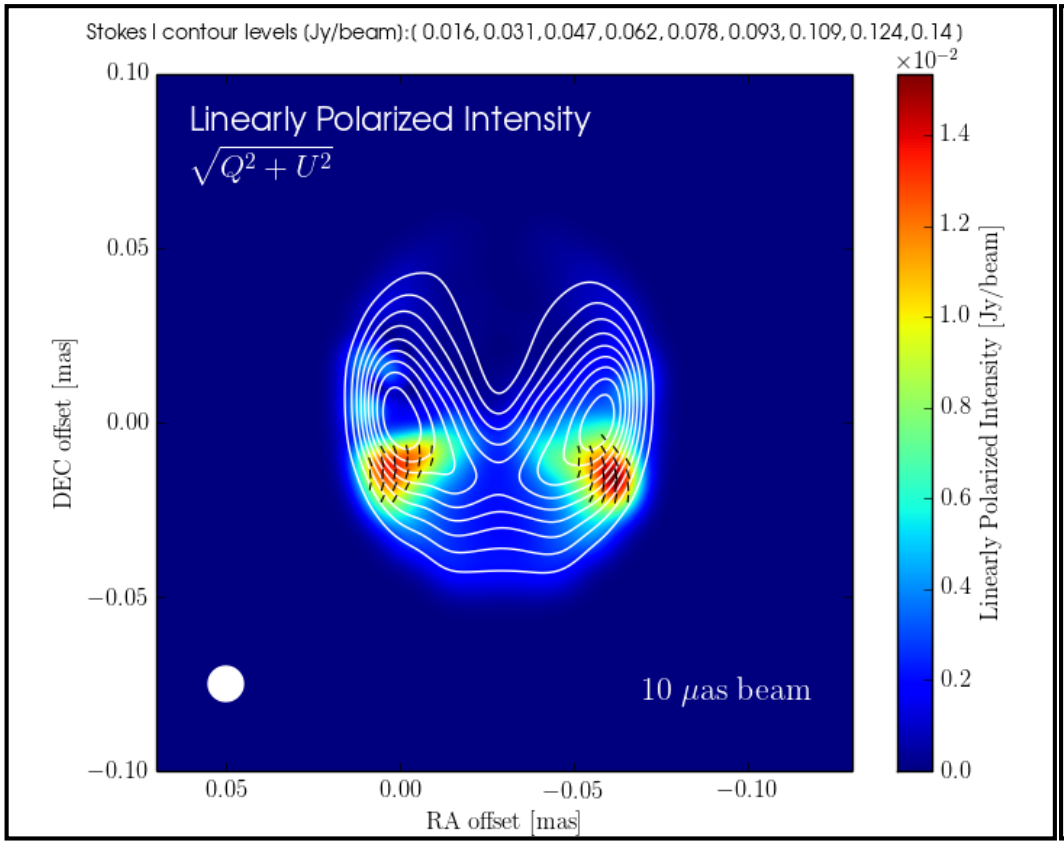

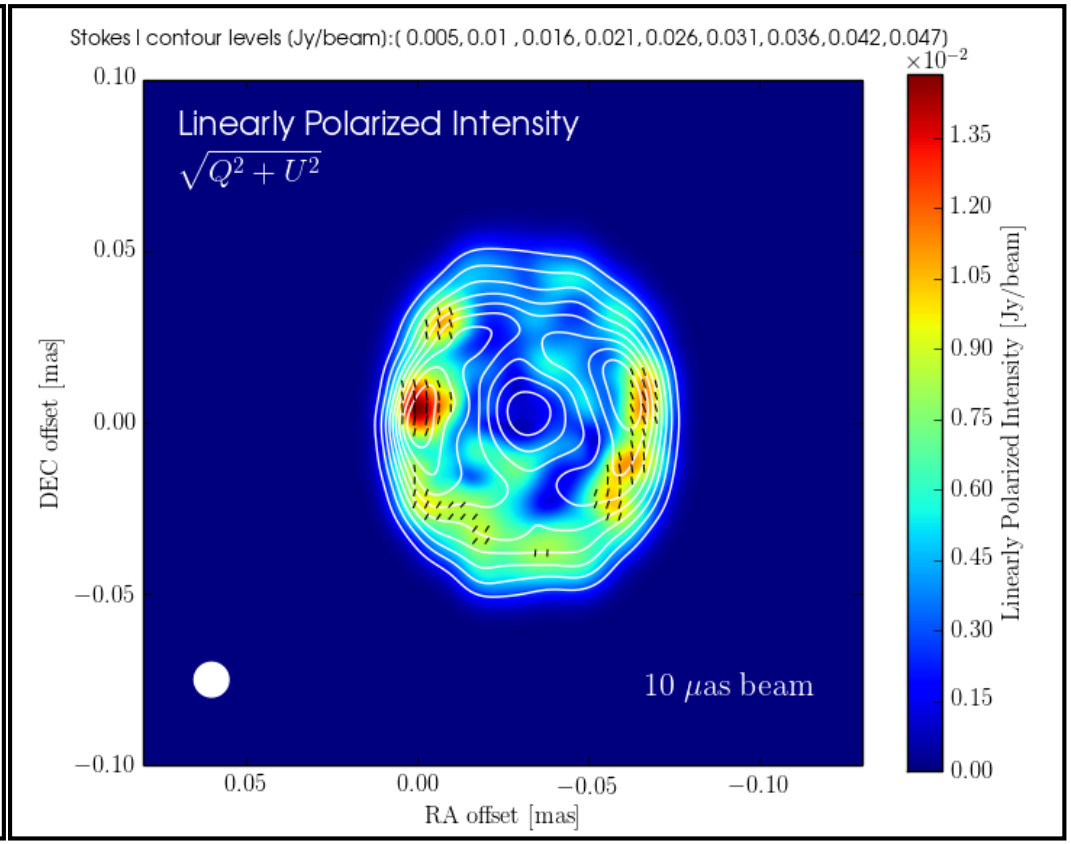

Helical Jet

Turbulent Jet

MacDonald & Marscher (in press)

TEMZ Imaging

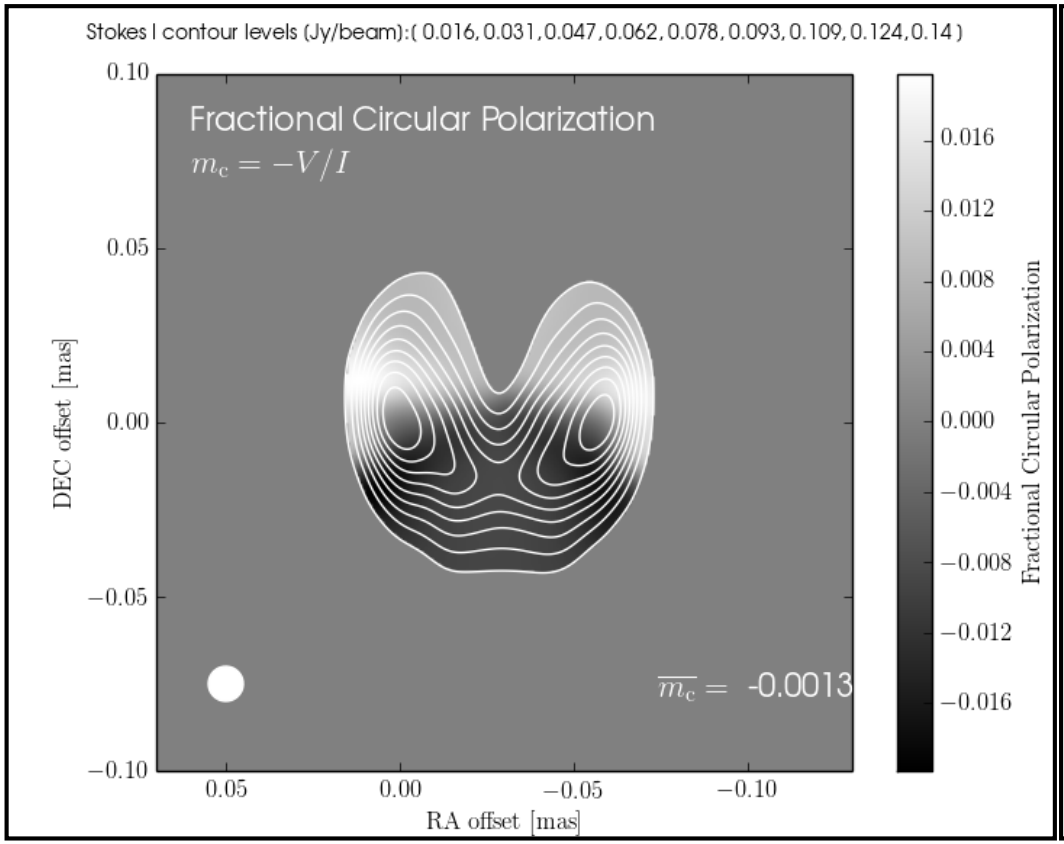

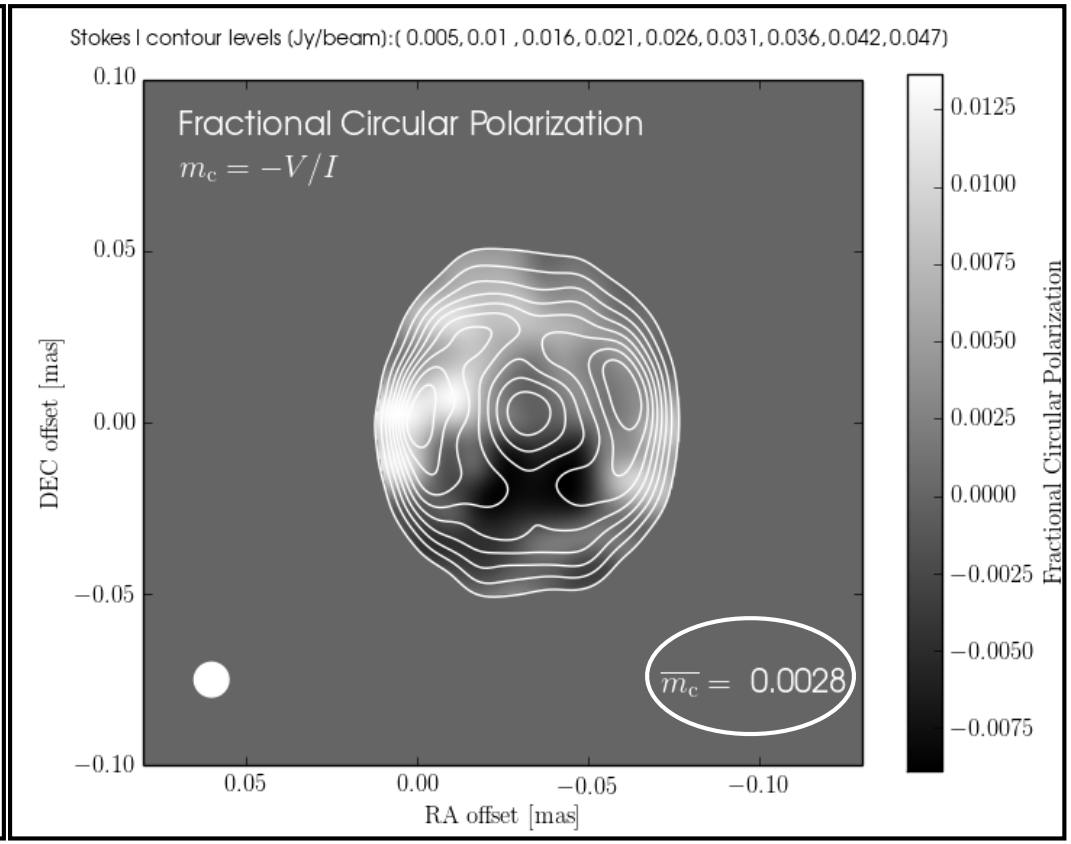

Helical Jet

Turbulent Jet

MacDonald & Marscher (in press)

TEMZ Light Curves

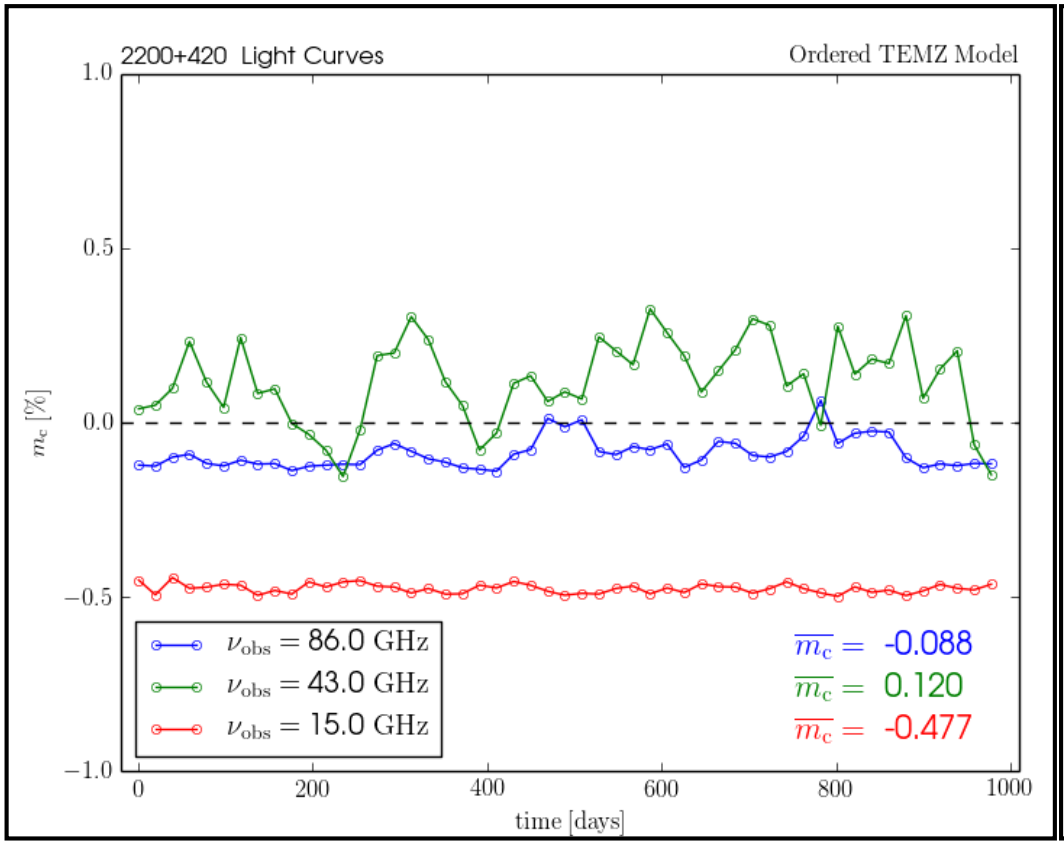

Helical Jet

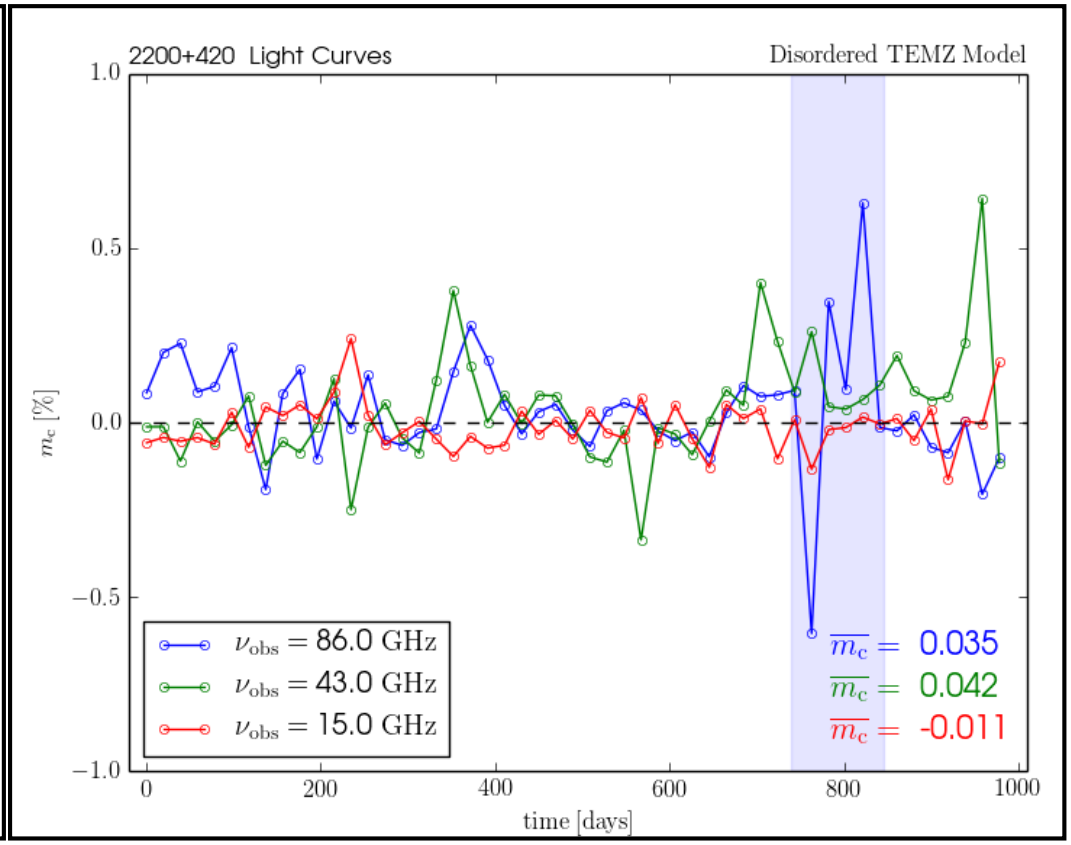

Turbulent Jet

MacDonald & Marscher (in press)

POLAMI

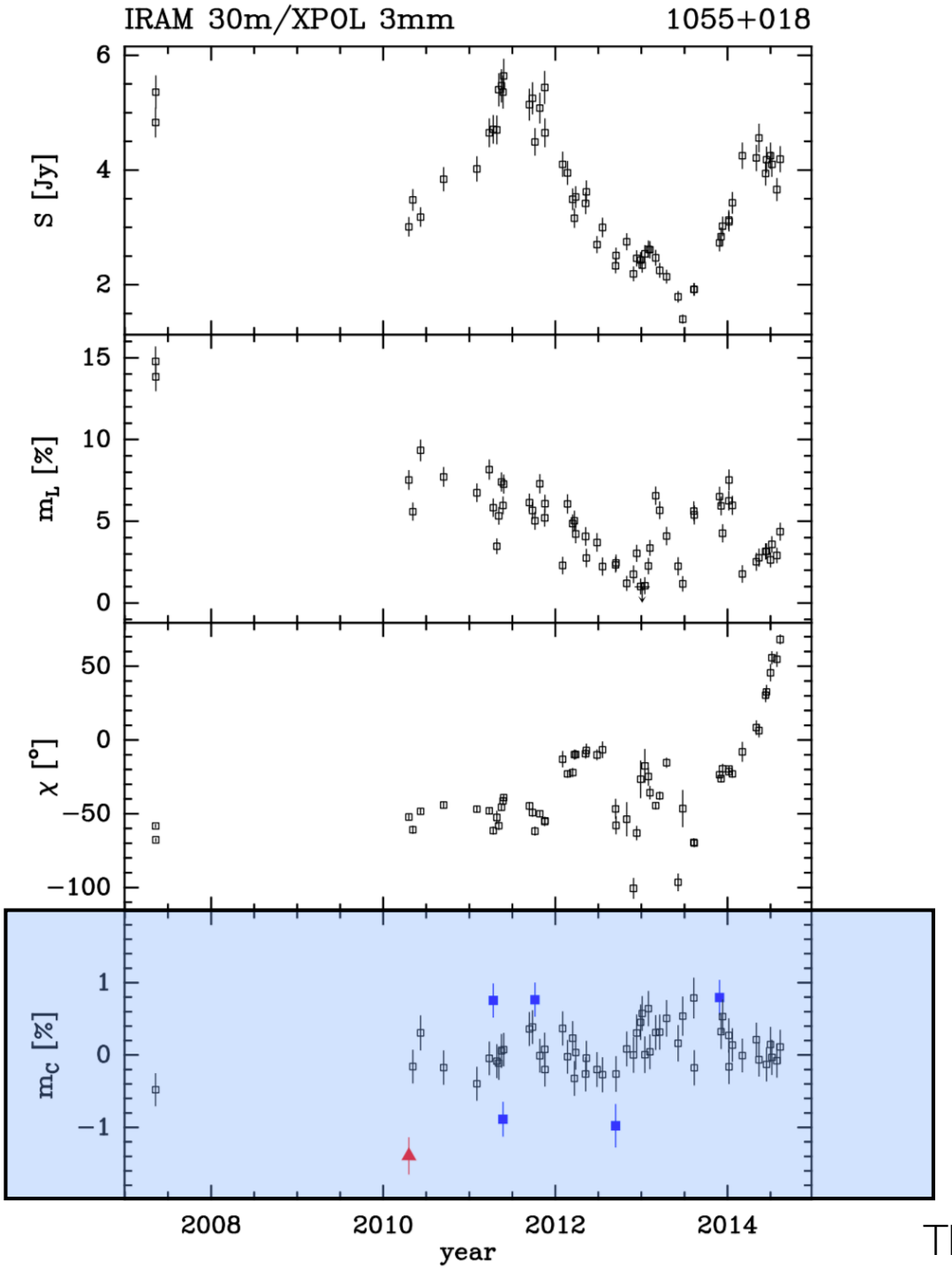

Thum et al. (2018)

F-GAMMA Program

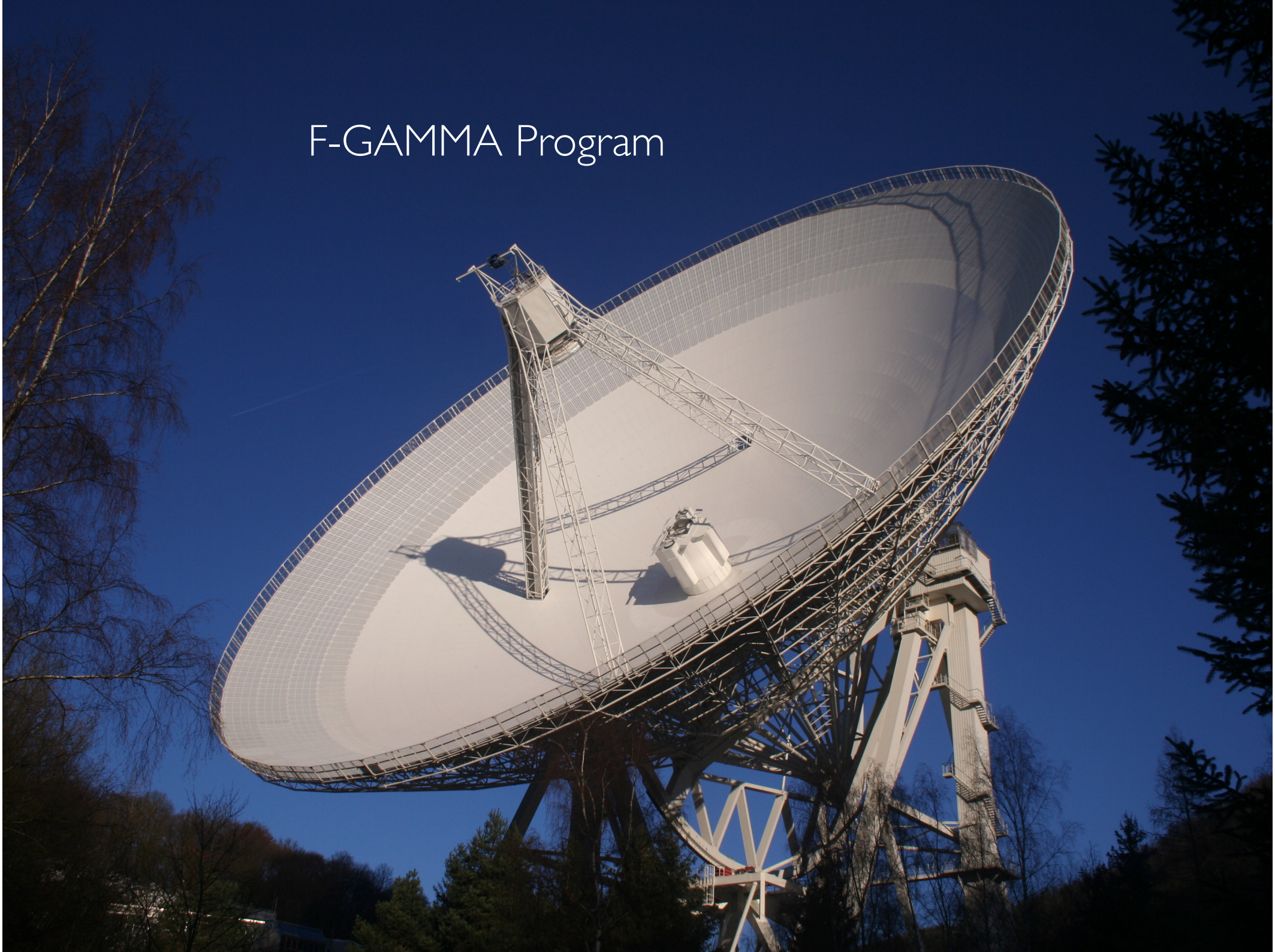

F-GAMMA

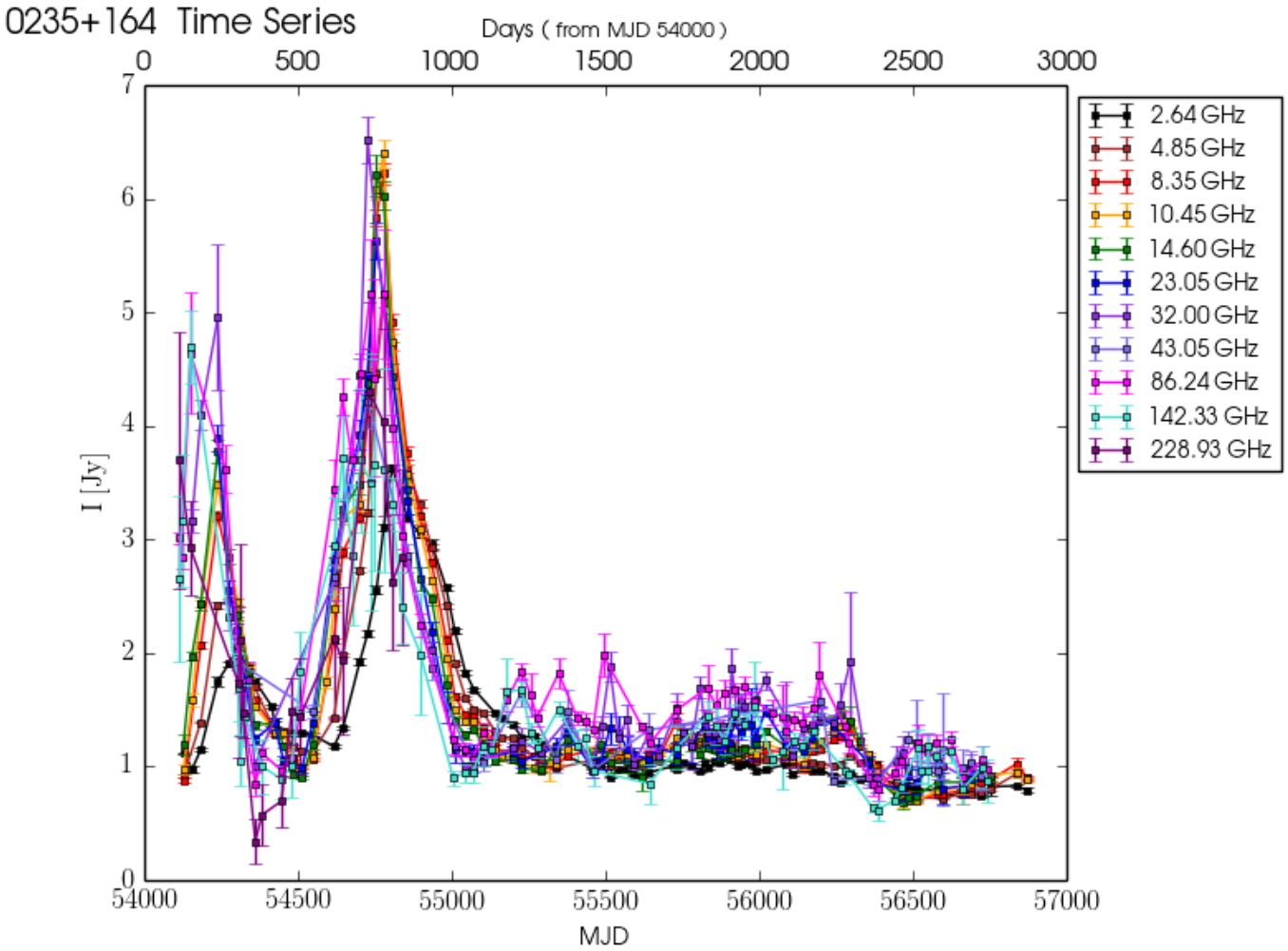

Angelakis (private communication)

F-GAMMA

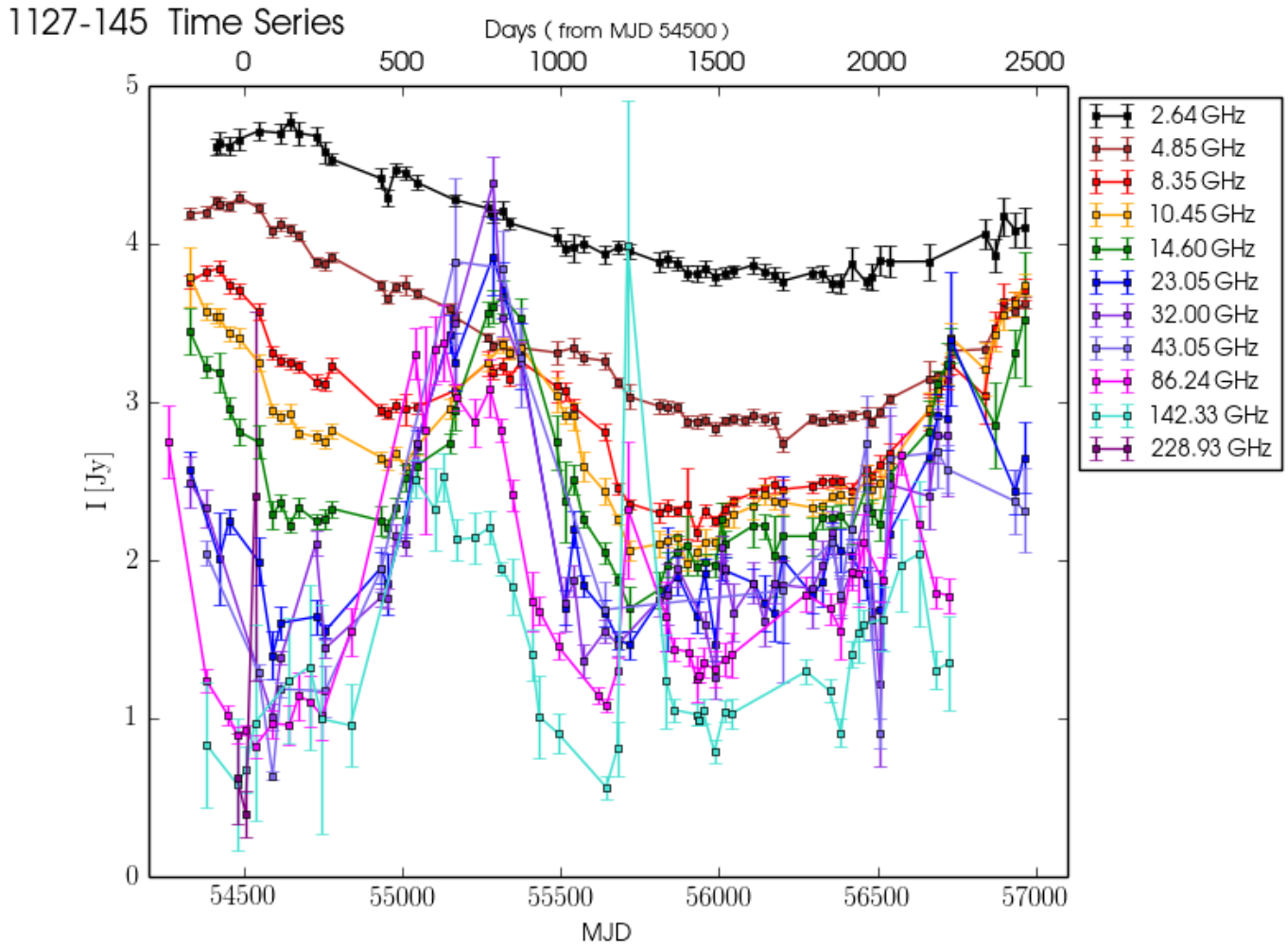

Angelakis (private communication)

TEMZ Light Curves

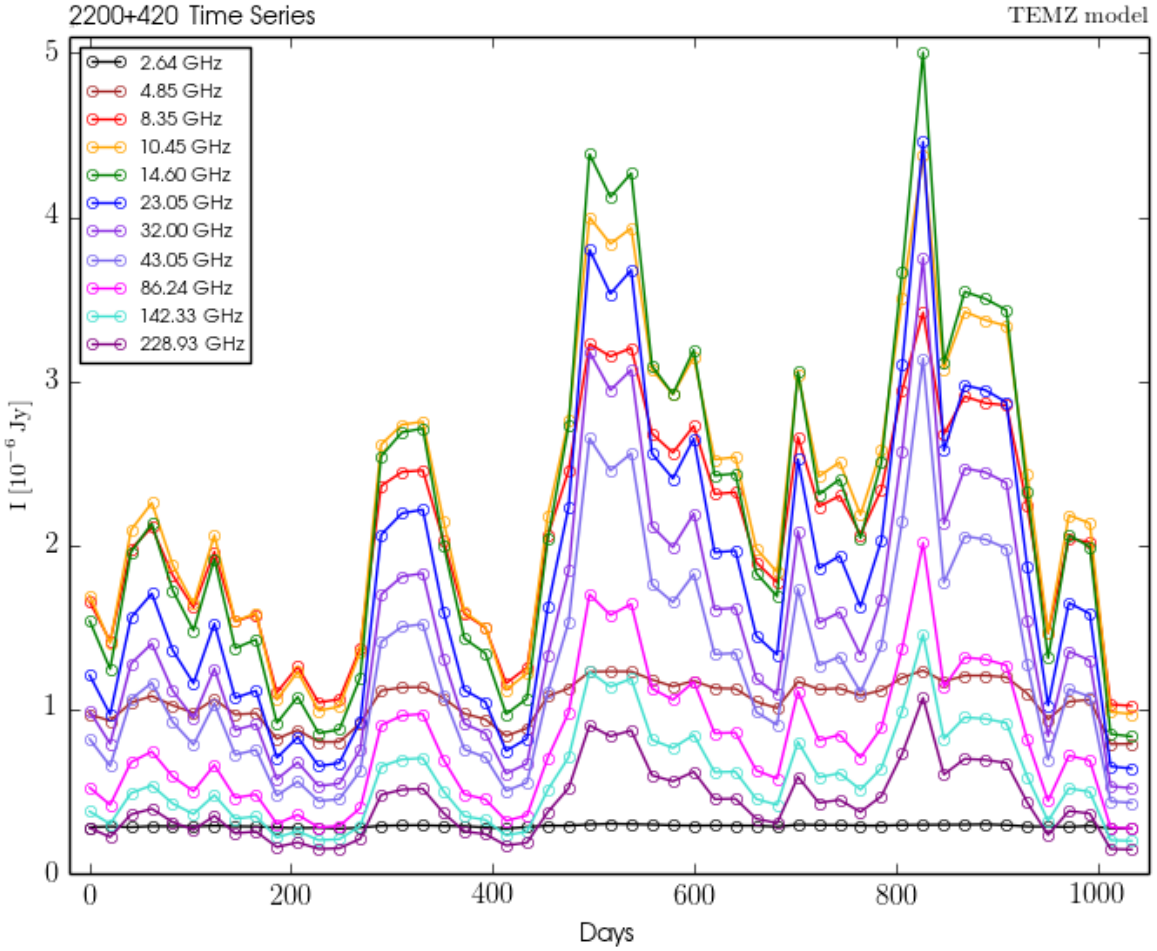

MacDonald, Angelakis, Myserlis et al. (in prep)

TEMZ Light Curves

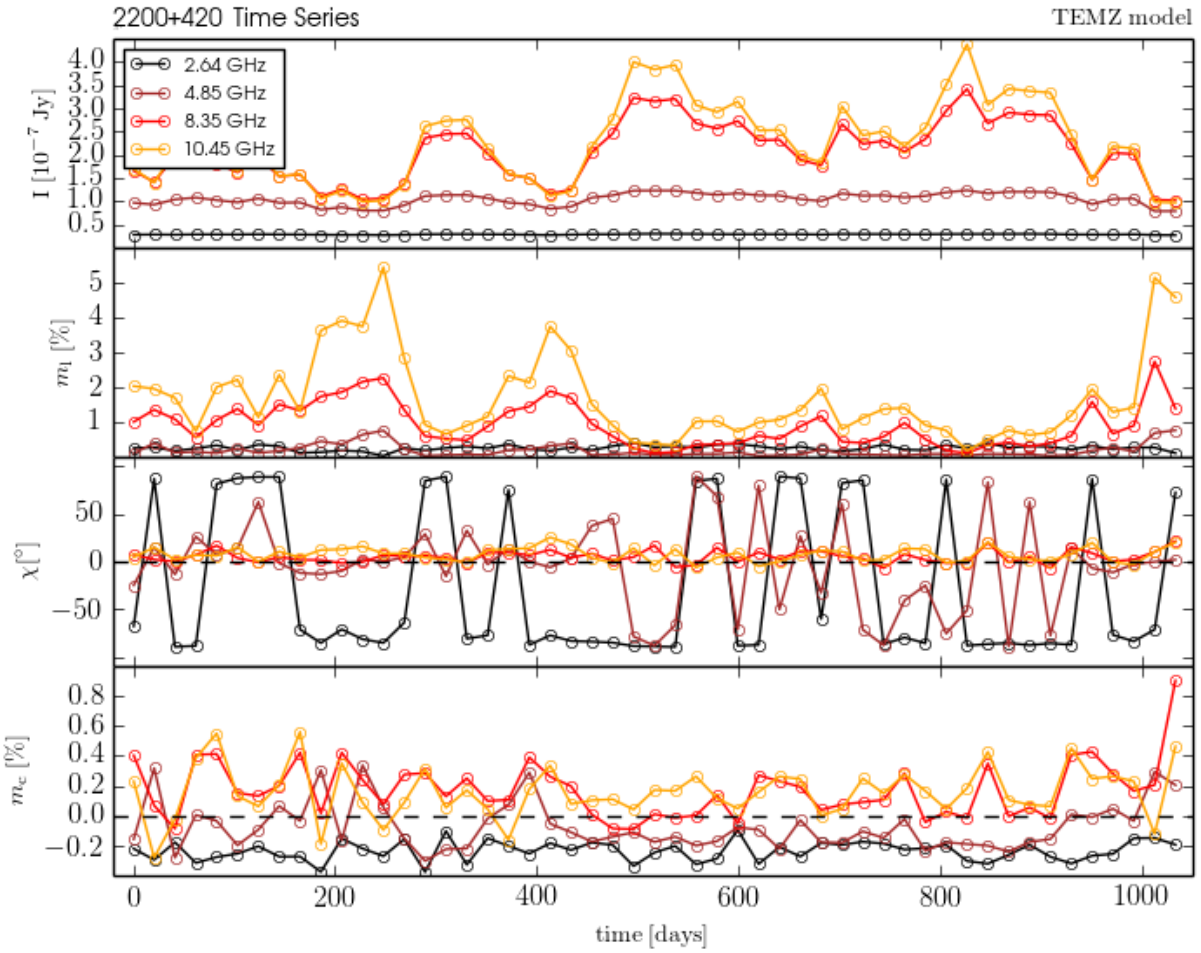

MacDonald, Angelakis, Myserlis et al. (in prep)

TEMZ Parameter Survey

TEMZ Model Parameters

Symbol	Description	Value
Z	Redshift	0.069
α	Optically thin spectral index	0.65
B	Mean magnetic field (G)	0.03
$-b$	Power-law slope of power spectrum	1.7
f_B	Ratio of energy densities u_e/u_B	0.1
$R_{\rm cell}$	Radius of TEMZ cells (pc)	0.004
$\gamma_{\rm max}$	Maximum electron energy	10000
$\gamma_{\rm min}$	Minimum electron energy	10
$\beta_{\mathbf{u}}$	Bulk laminar velocity of unshocked plasma	0.986
$\beta_{\mathbf{t}}$	Turbulent velocity of unshocked plasma	0.0
ζ	Angle between conical shock and jet axis	10°
$\theta_{\rm obs}$	Angle between jet axis and line of sight	6°
ϕ	Opening semi-angle of jet	6.8°
$z_{\rm MD}$	Distance of Mach disk from BH (pc)	1.0
$f_{\rm field}$	Ratio of ordered helical field to total field	0.1-1.0
ψ	Pitch angle of the helical field	45°
$n_{\rm step}$	Number of time steps	5000
$n_{\rm rad}$	Number of cells in jet cross-section	169

Synthetic GMVA Imaging of the TEMZ Model

3C 84

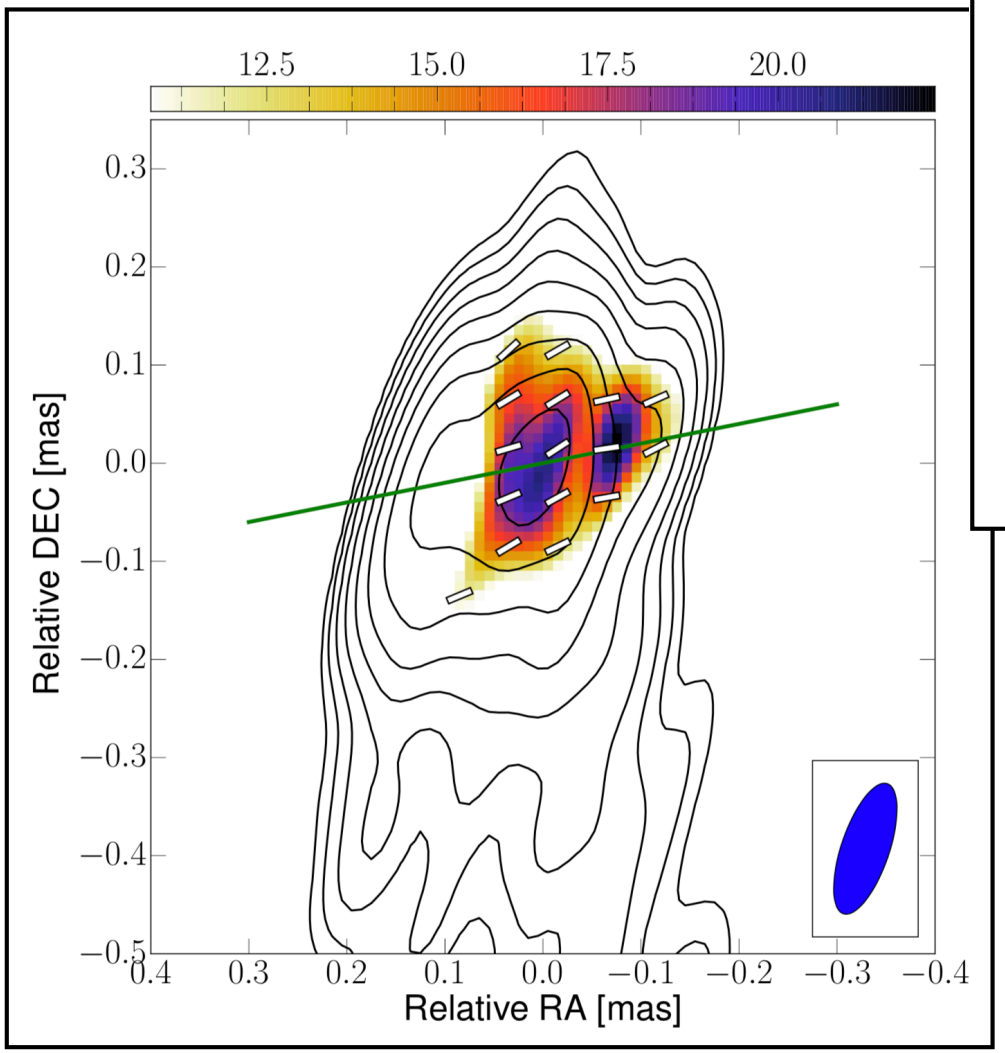

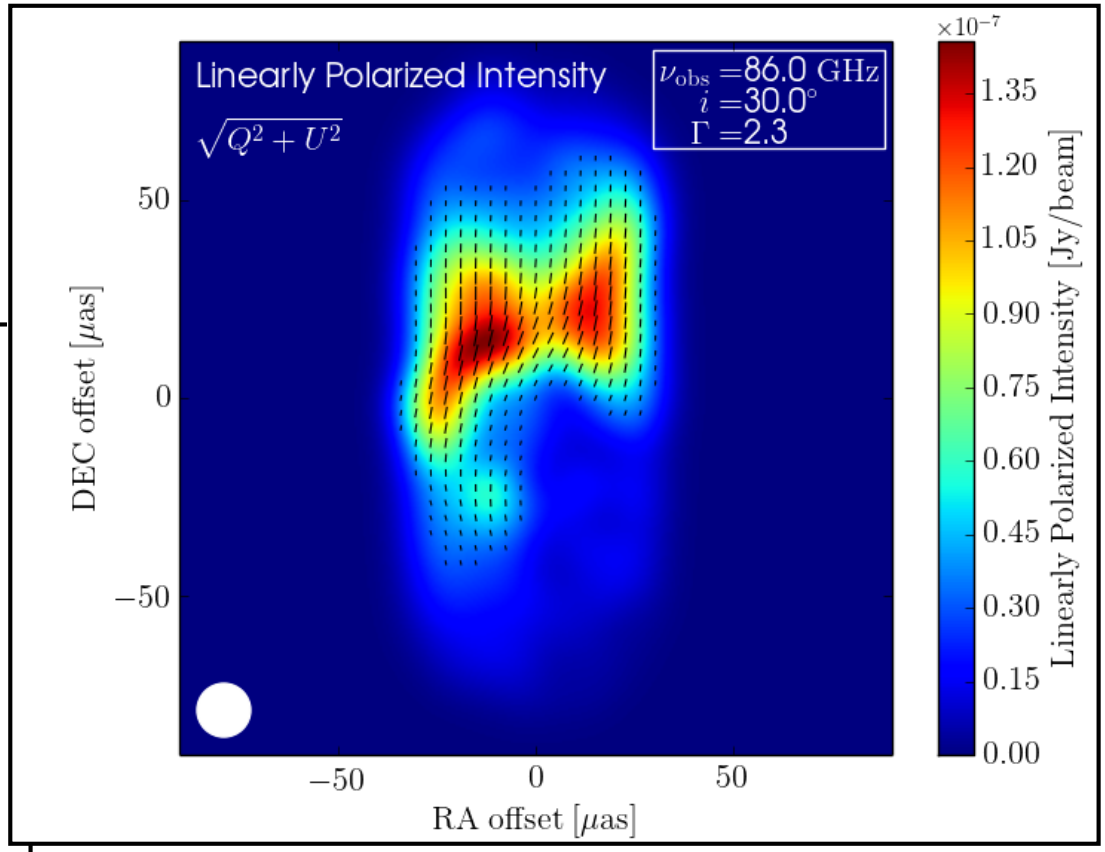

Kim et al. (submitted)

3C 84

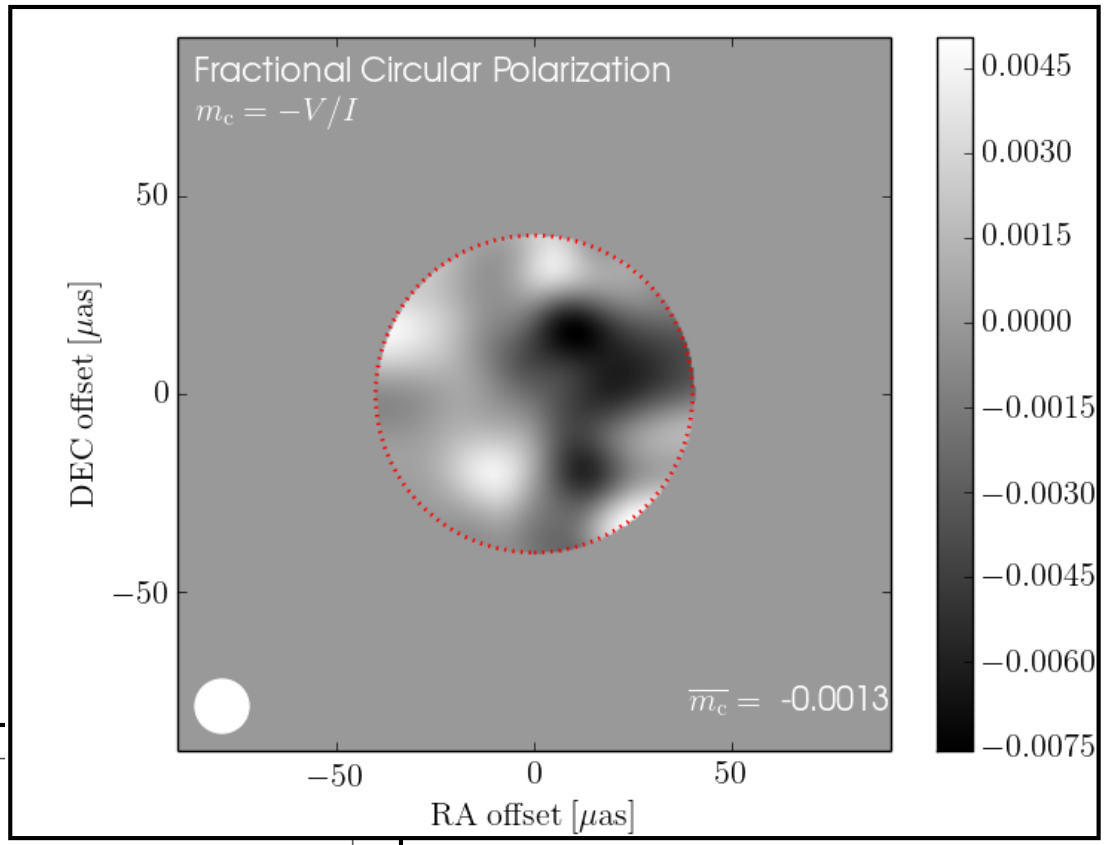

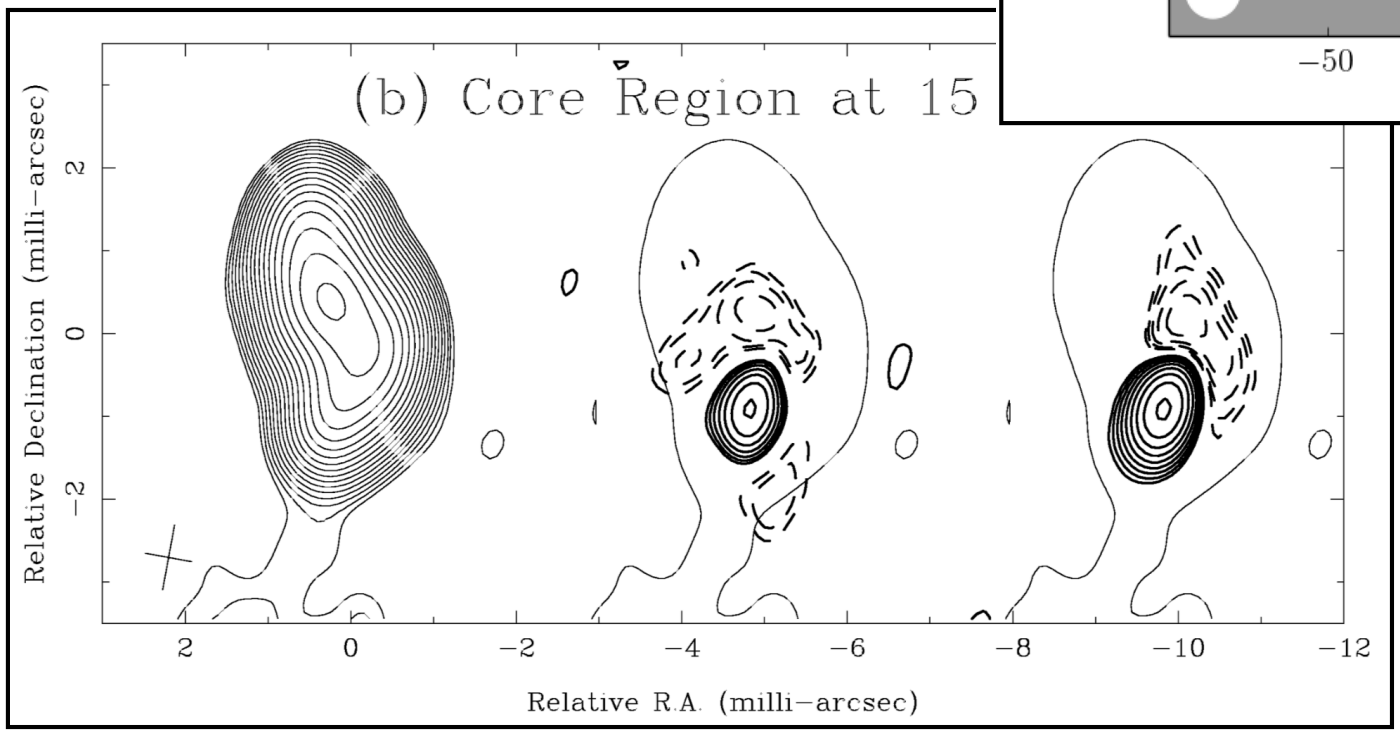

Homan & Wardle (2004)

PKS 1510-089

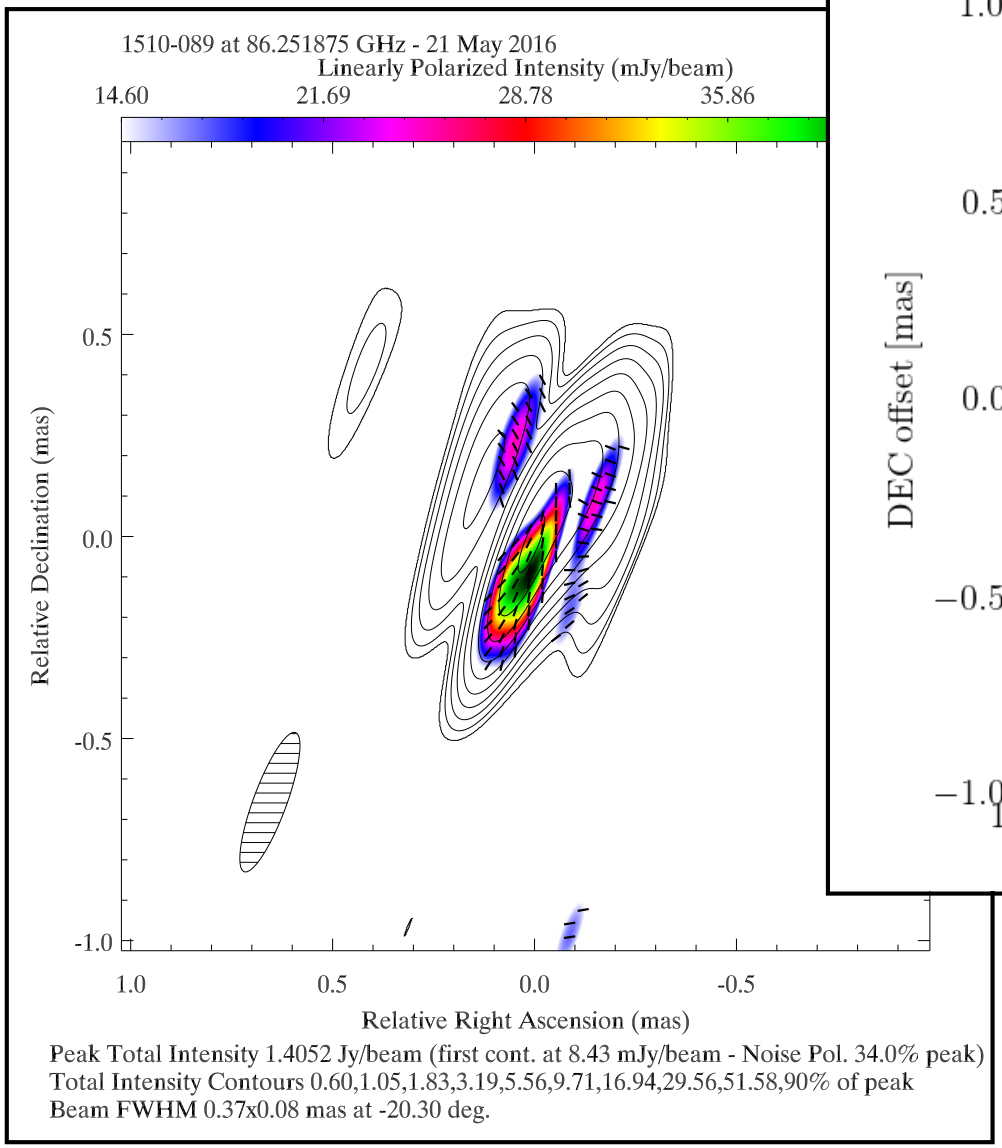

Casadio et al. (2017)

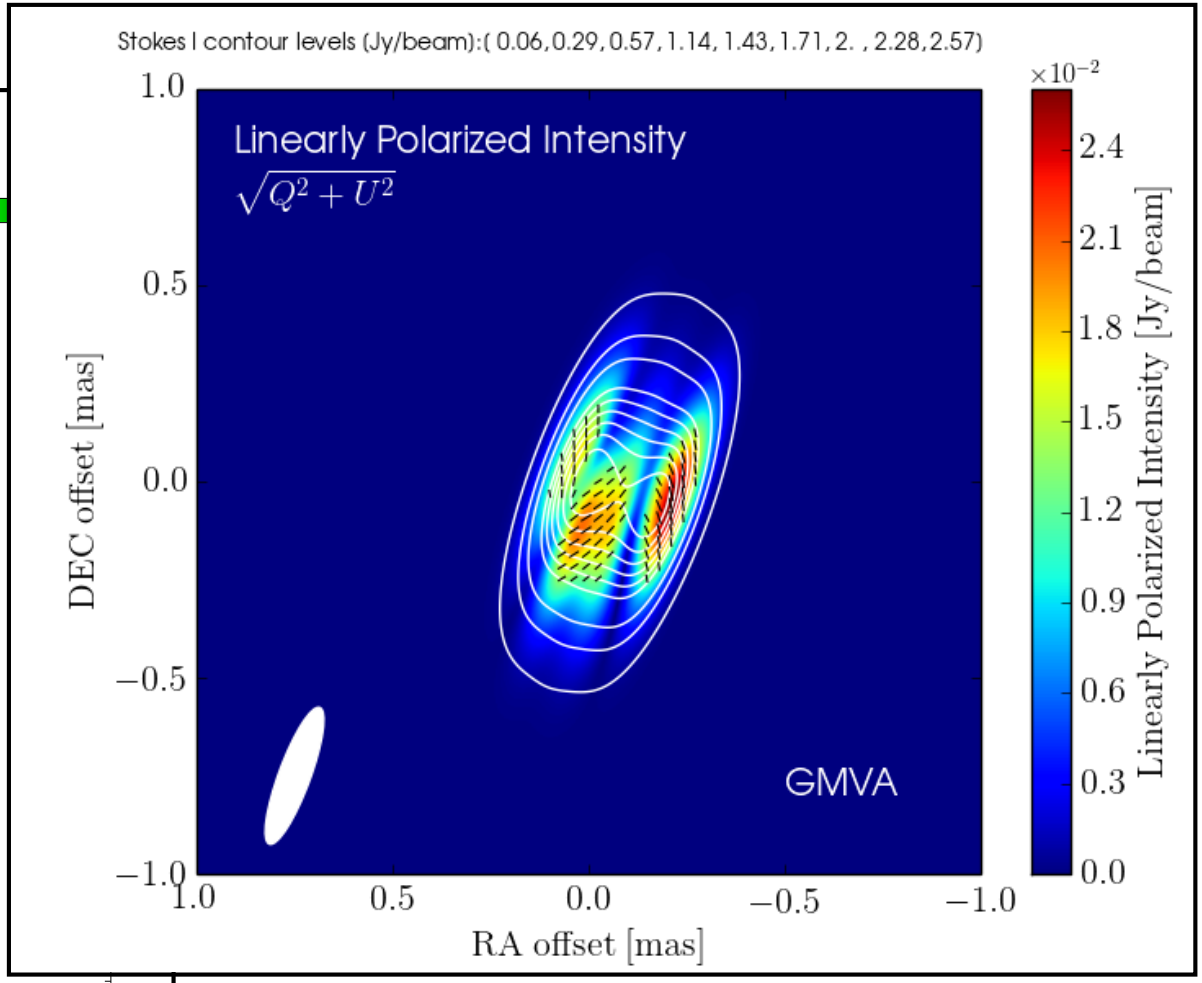

MacDonald, Casadio, et al. (in prep)

Ray-tracing Through a Relativistic PIC Jet Simulation

Particle-in-Cell (PIC)

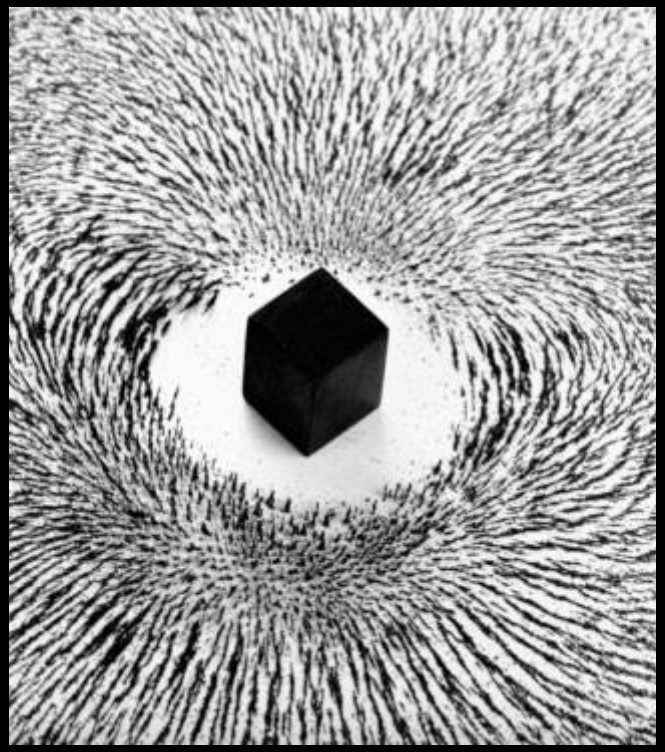

$$\frac{\partial}{\partial t} f + v \cdot \nabla_x f + \frac{q}{m}[E + v \times B] \cdot \nabla_v f = 0$$

Astronomy & Astrophysics manuscript no. draft1
April 26, 2018

Comparing the Micro to the Macro: Polarized Radiative Transfer Through 3-D Relativistic Particle-in-Cell Jet Simulations

N. R. MacDonald[1] and K.-I. Nishikawa[2]

[1] Max-Planck-Institut für Radioastronomie, Auf dem Hügel 69, D- 53121 Bonn, Germany
e-mail: nmacdona@mpifr-bonn.mpg.de
[2] Department of Physics, University of Alabama in Huntsville, ZP12, Huntsville, AL 35899, USA
e-mail: ken-ichi.nishikawa-1@nasa.gov

Received Month, Day, Year; accepted Month, Day, Year

ABSTRACT

Context. Relativistic extragalactic jets are collimated outflows of plasma that emanate from the centers of Active Galactic Nuclei (AGN). Despite decades of dedicated observation and study the underlying plasma composition of these outflows remains unknown.
Aims. Modern computational resources have allowed for increasingly sophisticated numerical jet simulations. Relativistic magnetohydrodynamic (RMHD) models are able to reproduce many of the observed macroscopic features of these outflows (e.g., recollimation shocks, jet sheaths, bow shocks, & enshrouding jet cocoons). The non-thermal synchrotron emission detected by Very Long Baseline Interferometric (VLBI) arrays, however, is a by-product of the microscopic physics occurring within the jet; physics that is not modeled directly in most RMHD codes. In this paper, we embark upon a study to discern the radiative differences between distinct plasma compositions within extragalactic jets using large scale relativistic Particle-in-Cell (PIC) simulations.
Methods. We make use of a polarized radiative transfer scheme to generate full Stokes imaging of two PIC jet simulations: one in which the jet is composed of an electron-proton plasma (i.e., a "normal plasma" jet) and the other in which the jet is composed of an electron-positron plasma (i.e., a "pair plasma" jet). We examine the differences in the level and morphology of the linear polarization (LP) and circular polarization (CP) emanating from these two jet models.
Results. We find that the level of fractional CP emanating from an electron-proton jet is several orders of magnitude larger than the level emanating from an electron-positron jet of similar speed and magnetic field strength. In addition, we find that the morphology of both the linearly and circularly polarized synchrotron emission is quite distinct between the two jet models. These results highlight the potential of future VLBI polarimetric imaging (on μas scales) to discern between normal plasma and pair plasma jet compositions. Placing a firm constraint on the plasma content of a relativistic extragalactic jet (via polarimetric imaging on the length scales presented in this paper) will have a profound impact on our understanding of the nature of jet "feedback" in AGN systems.

Key words. non-thermal radiative transfer – relativistic processes – polarization

1. Introduction

Relativistic jets are among the most persistent luminous sources in the cosmos. They are comprised of collimated streams of relativistic plasma that can extend up to thousands (and in some cases millions) of parsecs from their host galaxies. The current theoretical paradigm postulates that the ultimate source of energy powering these gargantuan outflows is the energy released from matter accreating onto a spinning supermassive black hole located in the nucleus of the host AGN.

With the advent of global (and now space based) VLBI we are able to probe the polarized emission emanating from the innermost reaches of relativistic extragalactic jets. Linearly and circularly polarized synchrotron radiation carry imprints of both the strength and orientation of the collimating magnetic field as well as the plasma content of the jet. Studying the nature of this radio/mm synchrotron emission can be used to infer the physical conditions of the jet mere parsecs from the central engine.

Particle-in-cell (PIC) codes solve Maxwell's equations at each numerical time step thus enabling a self-consistent treatment of the kinetic effects occurring within relativistic plasma simulations (e.g., plasma instabilities, jet shear, & magnetic reconnection). PIC simulations, however, are numerically intensive and this kinetic precision comes at the cost of small (relative to RMHD) simulation sizes. There exists, therefore, a synergy between PIC and RMHD jet modeling that must be utilized in order to gain a holistic understanding of the physics of relativistic jets. While RMHD models can simulate that large scale motions of a relativistic jet, PIC modeling can be used to investigate the small scale plasma and radiative processes occurring within the jet flow. It is these small scale processes that form a direct link to VLBI observations of polarized radio/mm jet emission.

In this paper, we study the radiative properties of two PIC simulations that represent small segments of much larger electron-proton ("normal plasma") and electron-positron ("pair plasma") jet flows. We make use of a polarized radiative transfer scheme that has been integrated into the ray-tracing code RADMC-3D. This ray-tracing package allows us to create synthetic full Stokes (I, Q, U, & V) images (as a post-process step) from our numerical PIC simulations.

This paper is organized as follows: In §2 we summarize the scaling relations used in our PIC models. In §3 we summarize the radiative transfer theory adopted in our study. In §4 we present the results of our ray-tracing calculations through a normal plasma and a pair plasma jet. Finally, in §5 we present our summary and conclusions. We adopt the following cosmological parameters: $H_o = 71$ km s^{-1} Mpc^{-1}, $\Omega_m = 0.27$, and $\Omega_\Lambda = 0.73$.

PIC Modeling

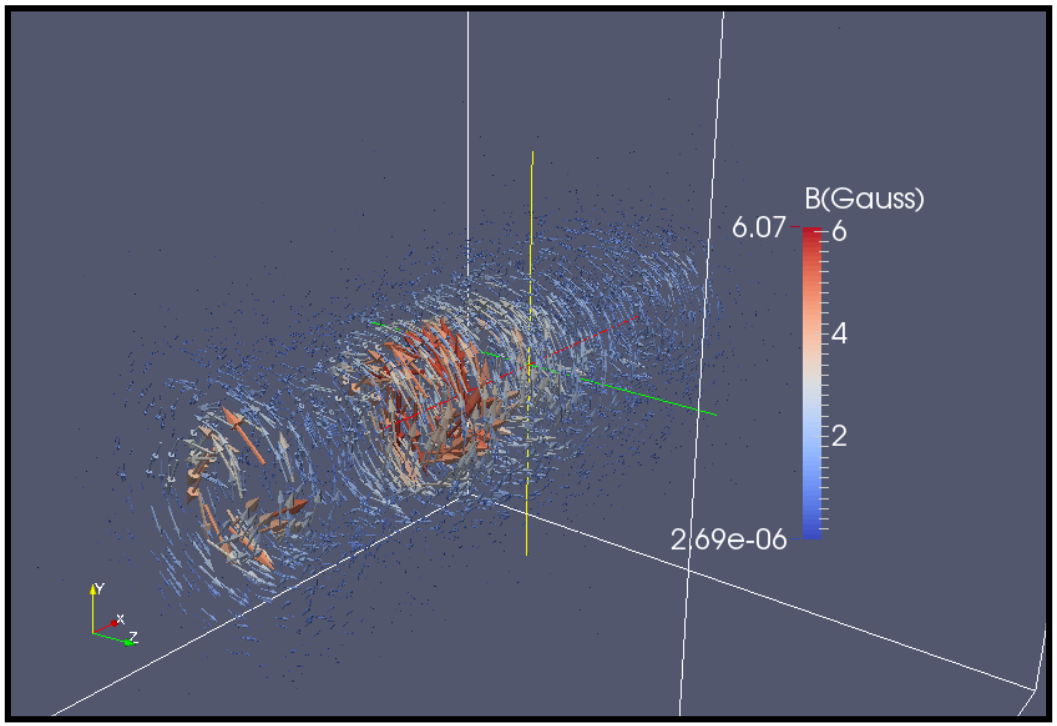

Normal Plasma Jet

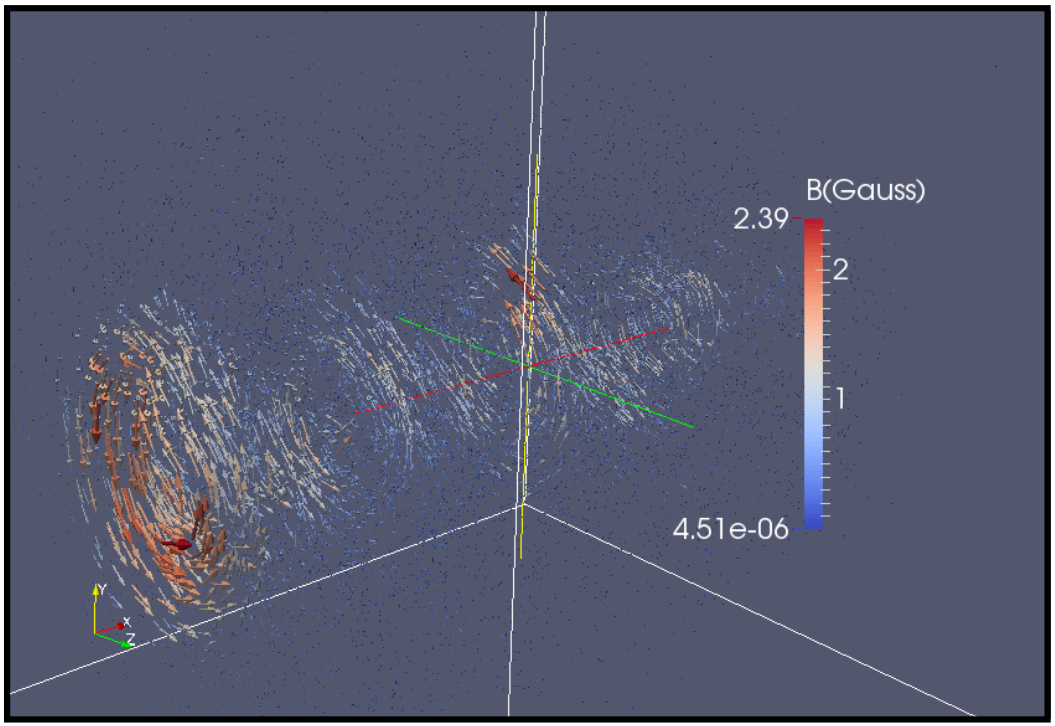

Pair Plasma Jet

MacDonald & Nishikawa (in prep)

PIC Imaging

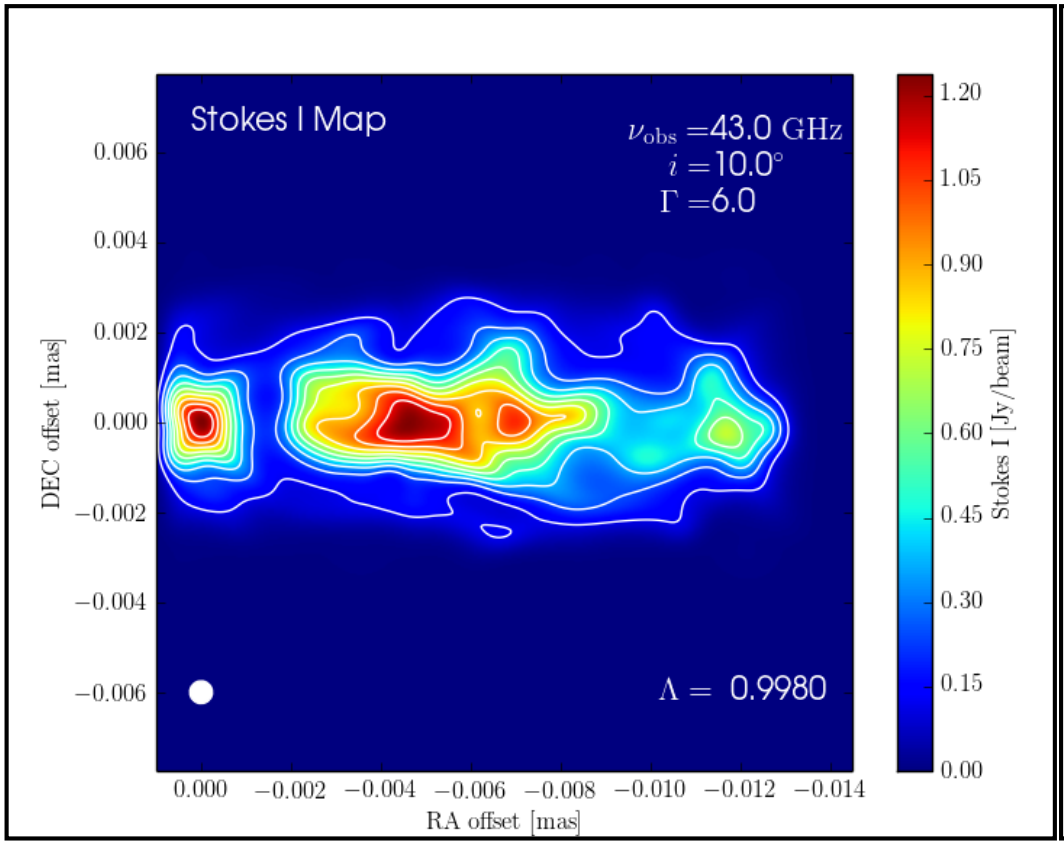

Normal Plasma Jet

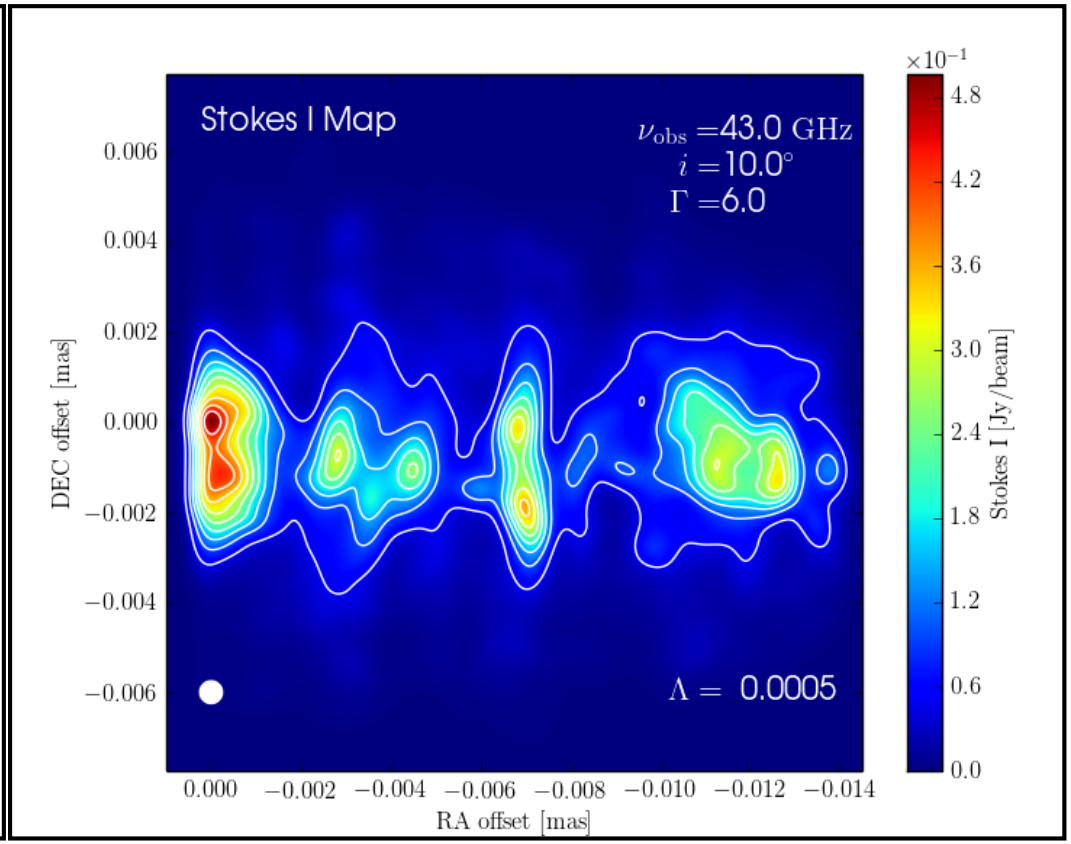

Pair Plasma Jet

MacDonald & Nishikawa (in prep)

PIC Imaging

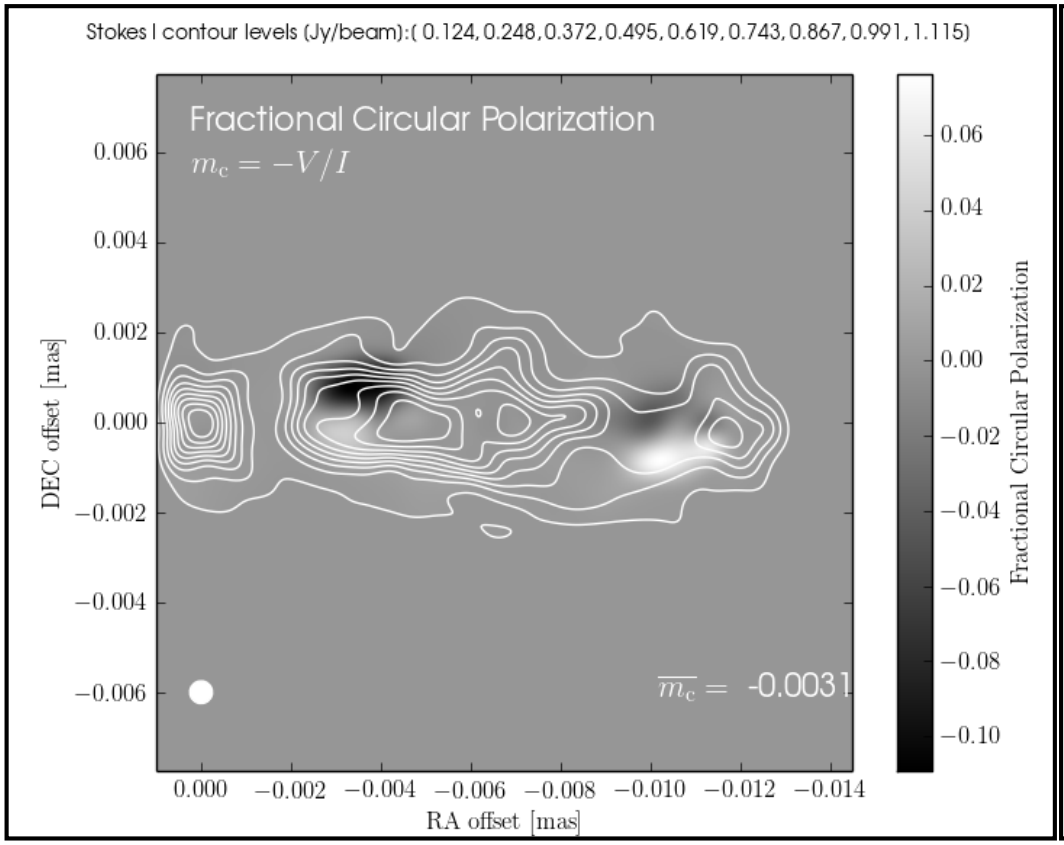

Normal Plasma Jet

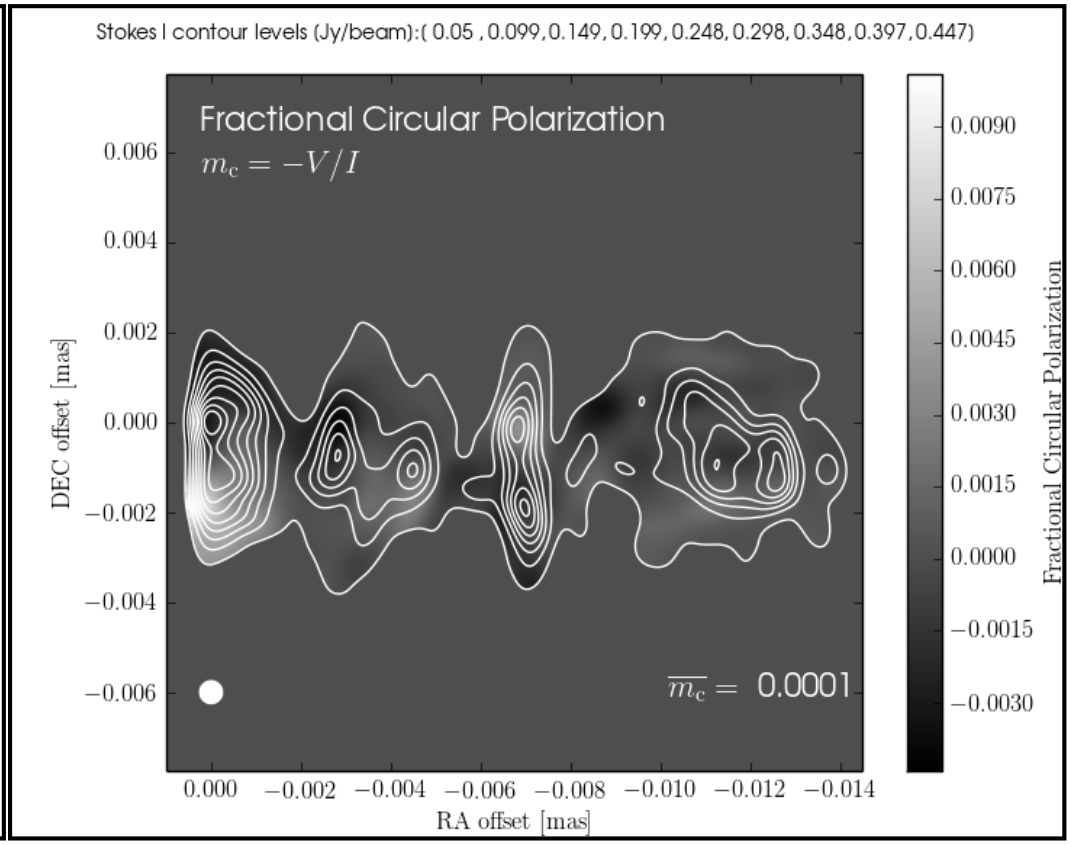

Pair Plasma Jet

MacDonald & Nishikawa (in prep)


Slow Light Interpolation
Ray
Jet

Ray-tracing Through an RMHD Jet Simulation

Relativistic Magnetohydrodynamics (RMHD)

$$\frac{\partial}{\partial t}\begin{pmatrix} D \\ \mathbf{m} \\ E \\ \mathbf{B} \end{pmatrix} + \nabla \cdot \begin{pmatrix} D\mathbf{v} \\ w_t\gamma^2\mathbf{v}\mathbf{v} - \mathbf{b}\mathbf{b} + |p_t \\ \mathbf{m} \\ \mathbf{v}\mathbf{B} - \mathbf{B}\mathbf{v} \end{pmatrix}^T = 0$$

A PARTICLE MODULE FOR THE PLUTO CODE: I - AN IMPLEMENTATION OF THE MHD-PIC EQUATIONS

A. Mignone
Physics Department, University of Turin, via Pietro Giuria 1 (10125) Torino, Italy

G. Bodo
INAF, Osservatorio Astrofisico di Torino, Strada Osservatorio 20, Pino Torinese 10025, Italy

B. Vaidya
Centre of Astronomy, Indian Institute of Technology Indore, Khandwa Road, Simrol , Indore 453552, India

and

G. Mattia
Physics Department, University of Turin, via Pietro Giuria 1 (10125) Torino, Italy

Draft version April 6, 2018

ABSTRACT

We describe an implementation of a particle physics module available for the PLUTO code, appropriate for the dynamical evolution of a plasma consisting of a thermal fluid and a non-thermal component represented by relativistic charged particles, or cosmic rays (CR). While the fluid is approached using standard numerical schemes for magnetohydrodynamics, CR particles are treated kinetically using conventional Particle-In-Cell (PIC) techniques.

The module can be used to describe either test particles motion in the fluid electromagnetic field or to solve the fully coupled MHD-PIC system of equations with particle backreaction on the fluid as originally introduced by Bai et al. (2015). Particle backreaction on the fluid is included in the form of momentum-energy feedback and by introducing the CR-induced Hall term in Ohm's law. The hybrid MHD-PIC module can be employed to study CR kinetic effects on scales larger than the (ion) skin depth provided the Larmor gyration scale is properly resolved. When applicable, this formulation avoids to resolve microscopic scales offering a substantial computational saving with respect to PIC simulations.

We present a fully-conservative formulation which is second-order accurate in time and space and extends to either Runge-Kutta (RK) or corner-transport-upwind (CTU) time-stepping schemes (for the fluid) while a standard Boris integrator is employed for the particles. For highly-energetic relativistic CRs and in order to overcome the time step restriction a novel sub-cycling strategy that retains second-order accuracy in time is presented. Numerical benchmarks and applications including Bell instability, diffusive shock acceleration and test particle acceleration in reconnecting layers are discussed.

Subject headings: plasmas – magnetohydrodynamics (MHD) – methods: numerical – acceleration of particles – shock waves – instabilities

Bonn Correlator

RMHD Modeling

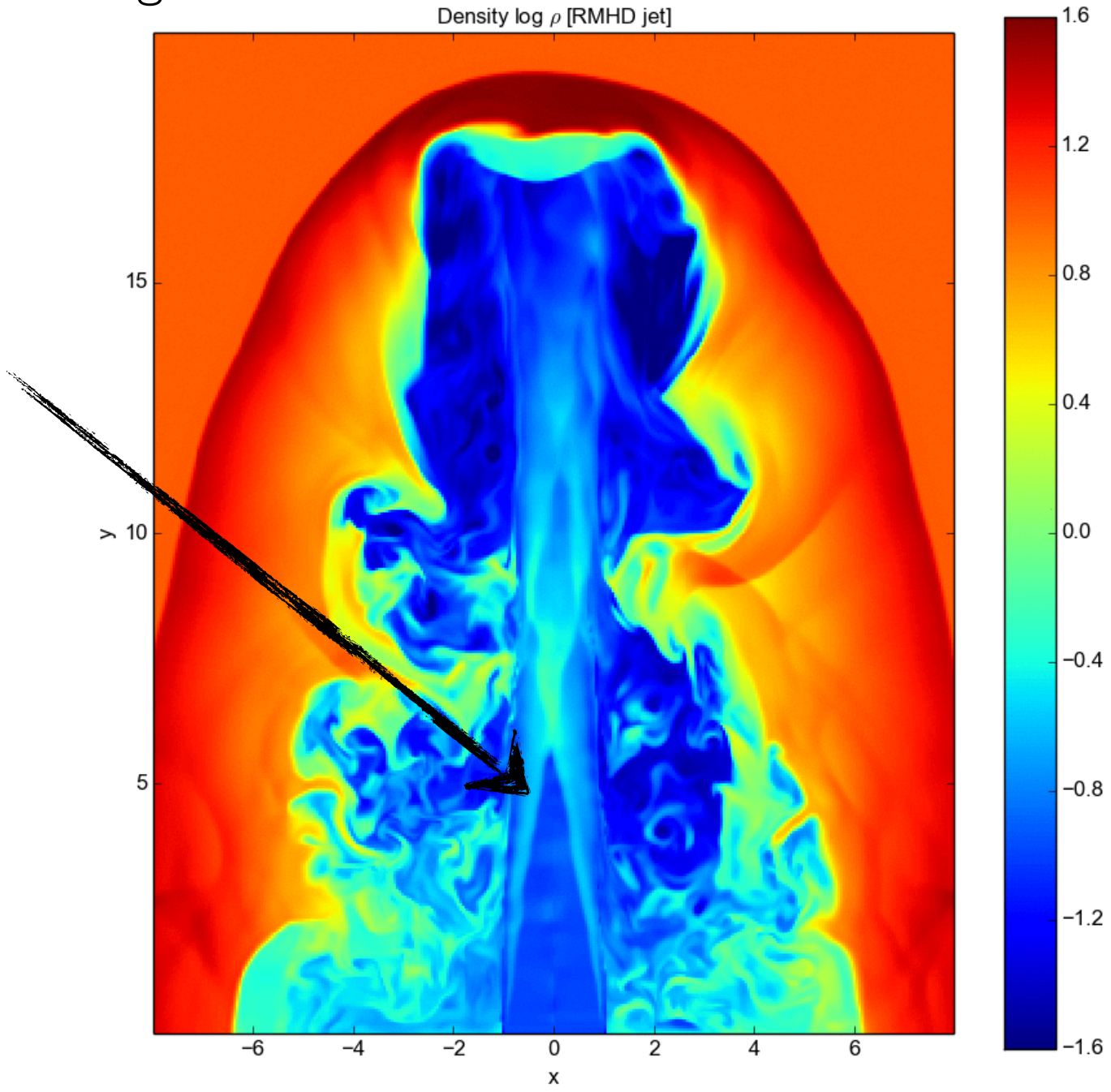

RMHD Modeling

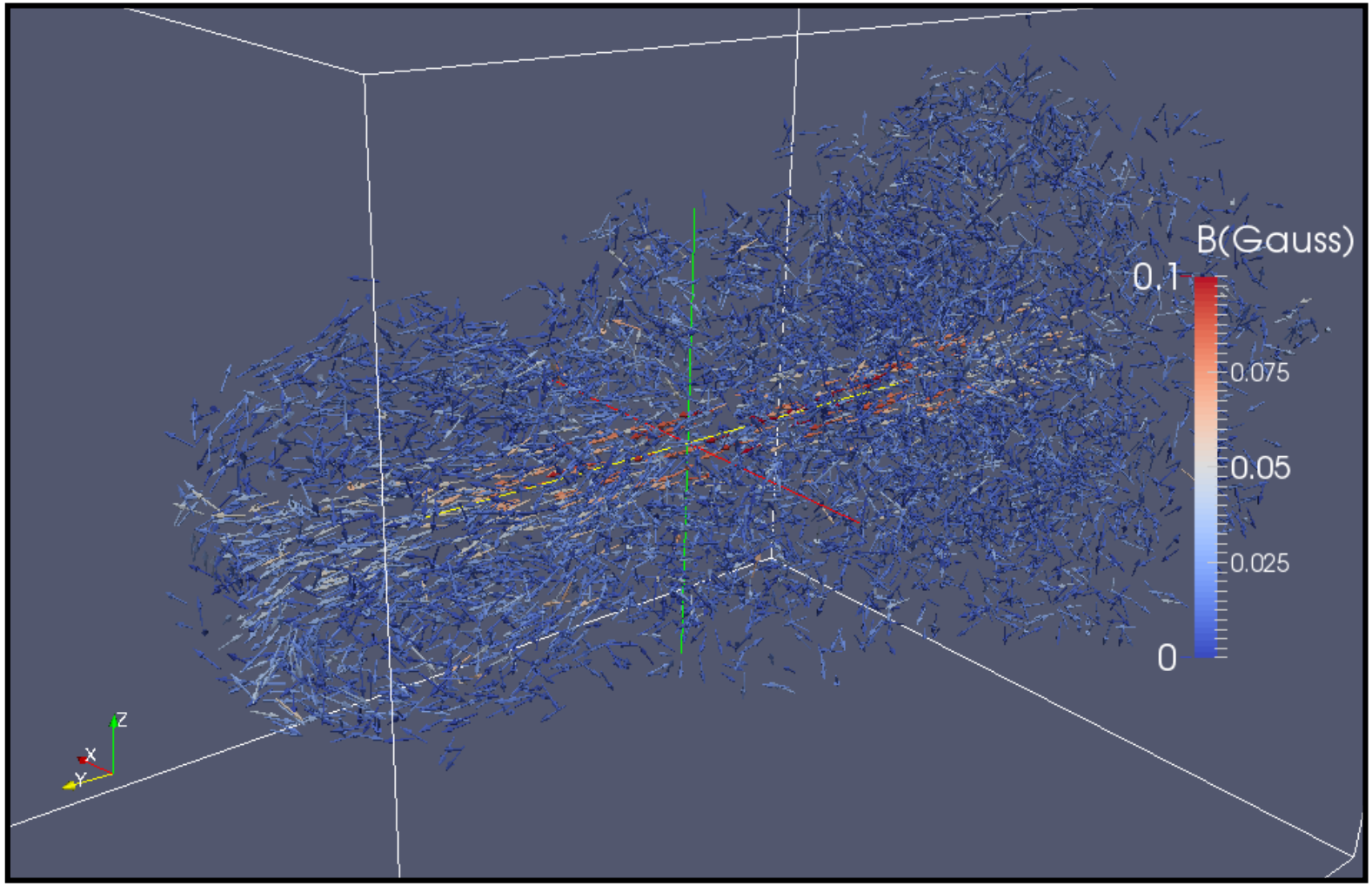

Poloidal Jet

RMHD Modeling

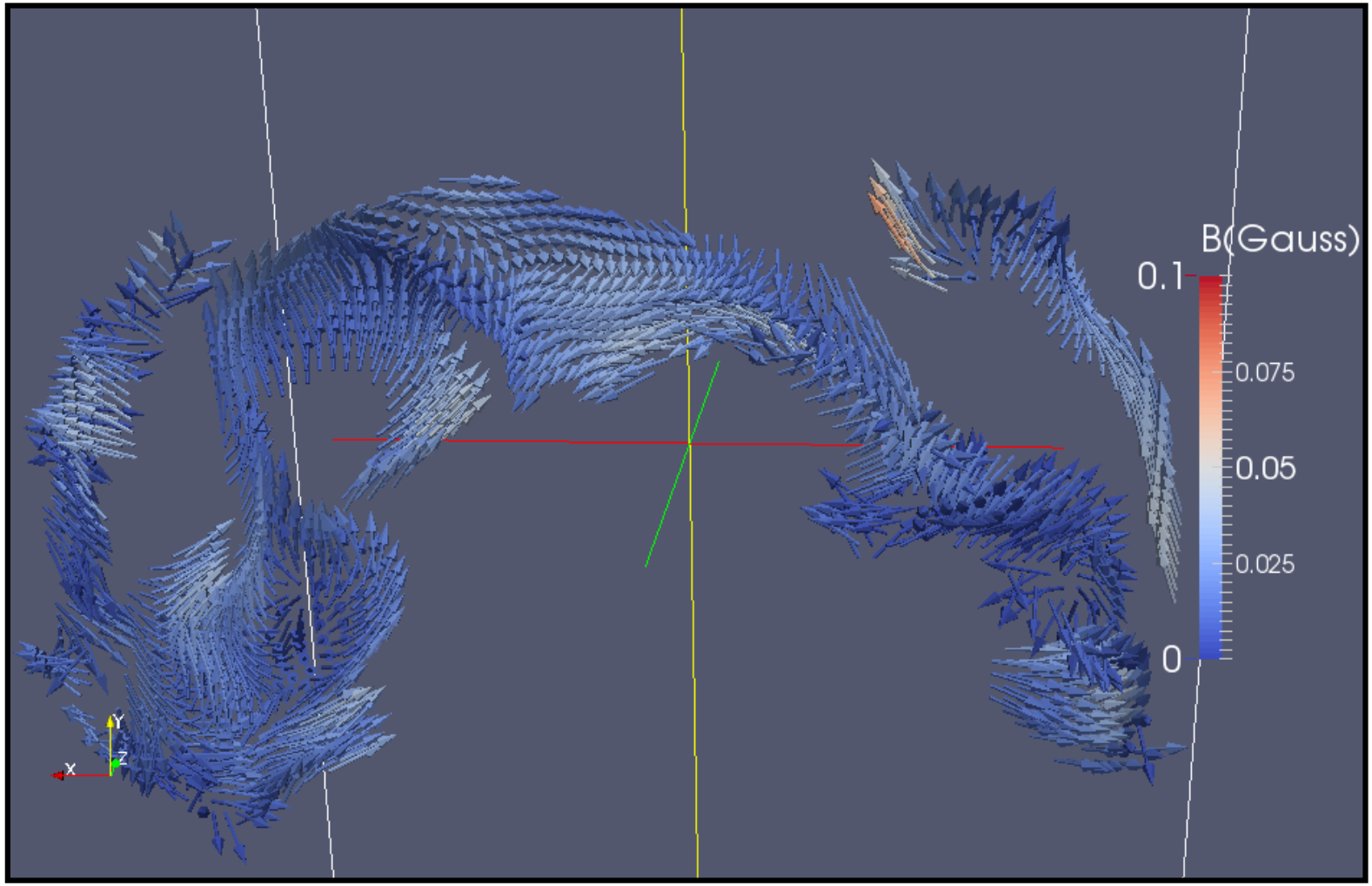

Poloidal Jet

RMHD Modeling

From the Macro…

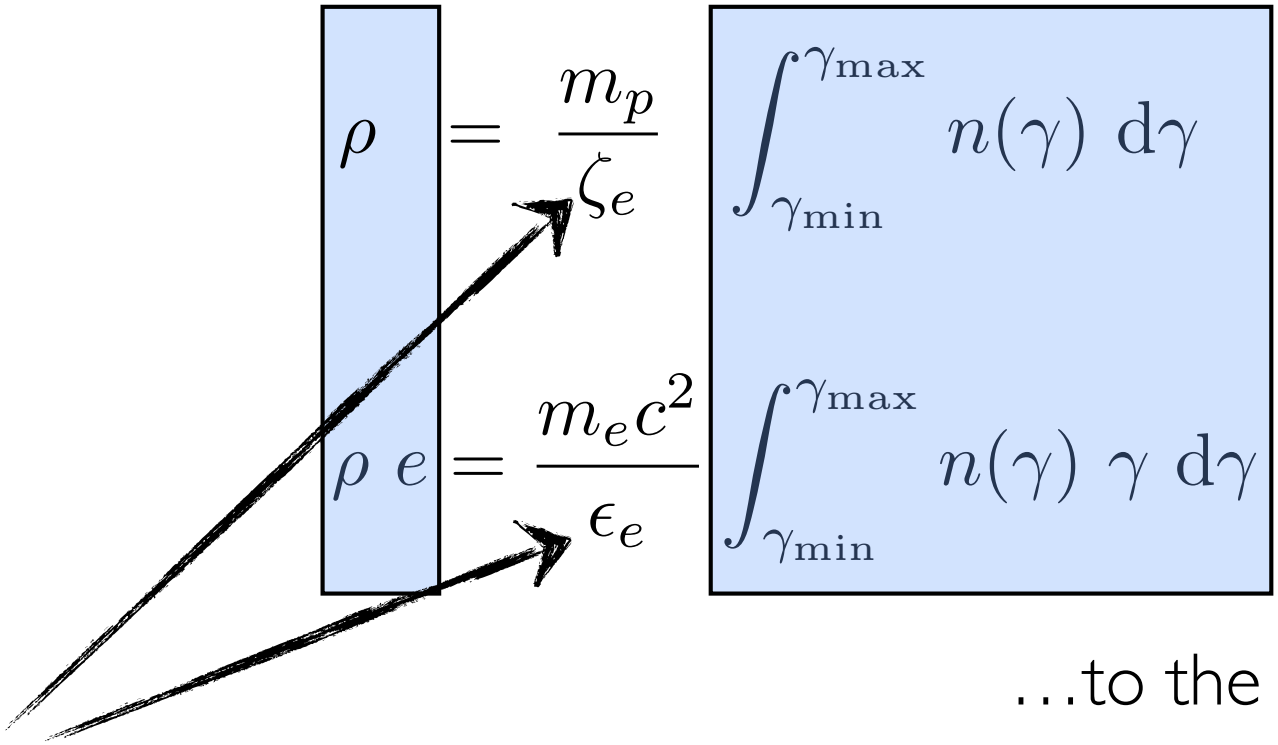

…to the Micro

Fromm et al. (2016)

RMHD Imaging

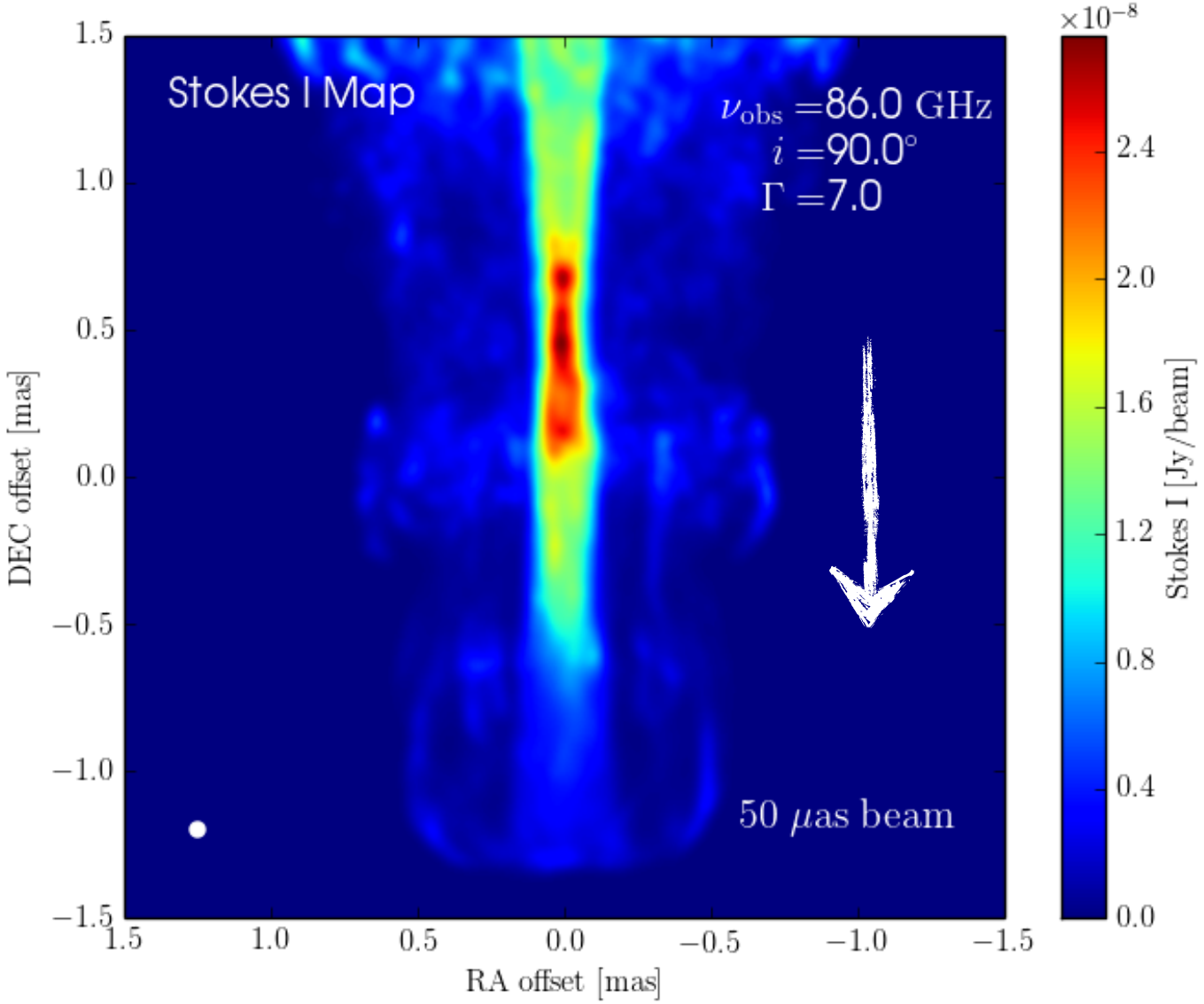

MacDonald (in prep)

RMHD Imaging

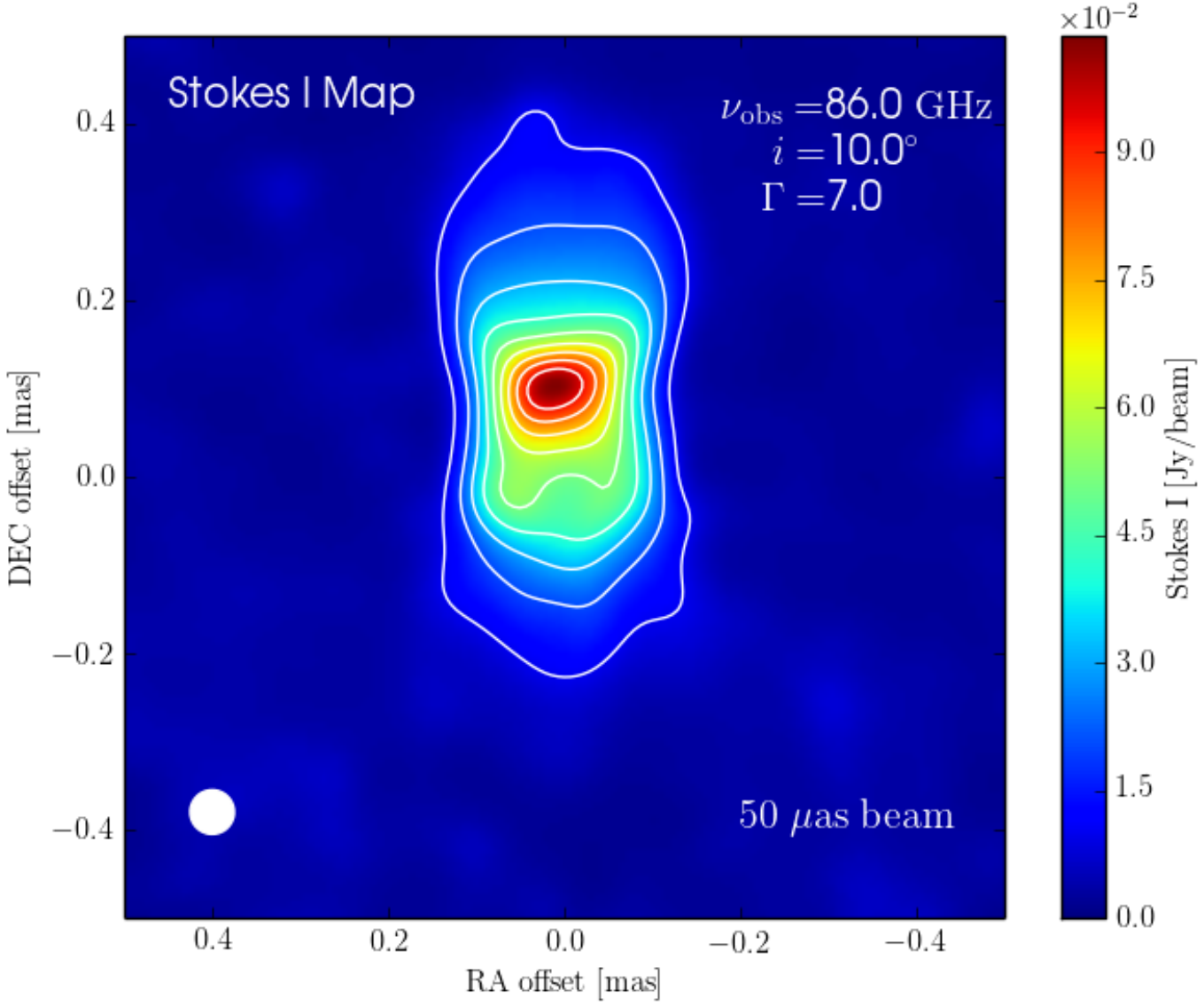

MacDonald (in prep)

RMHD Imaging

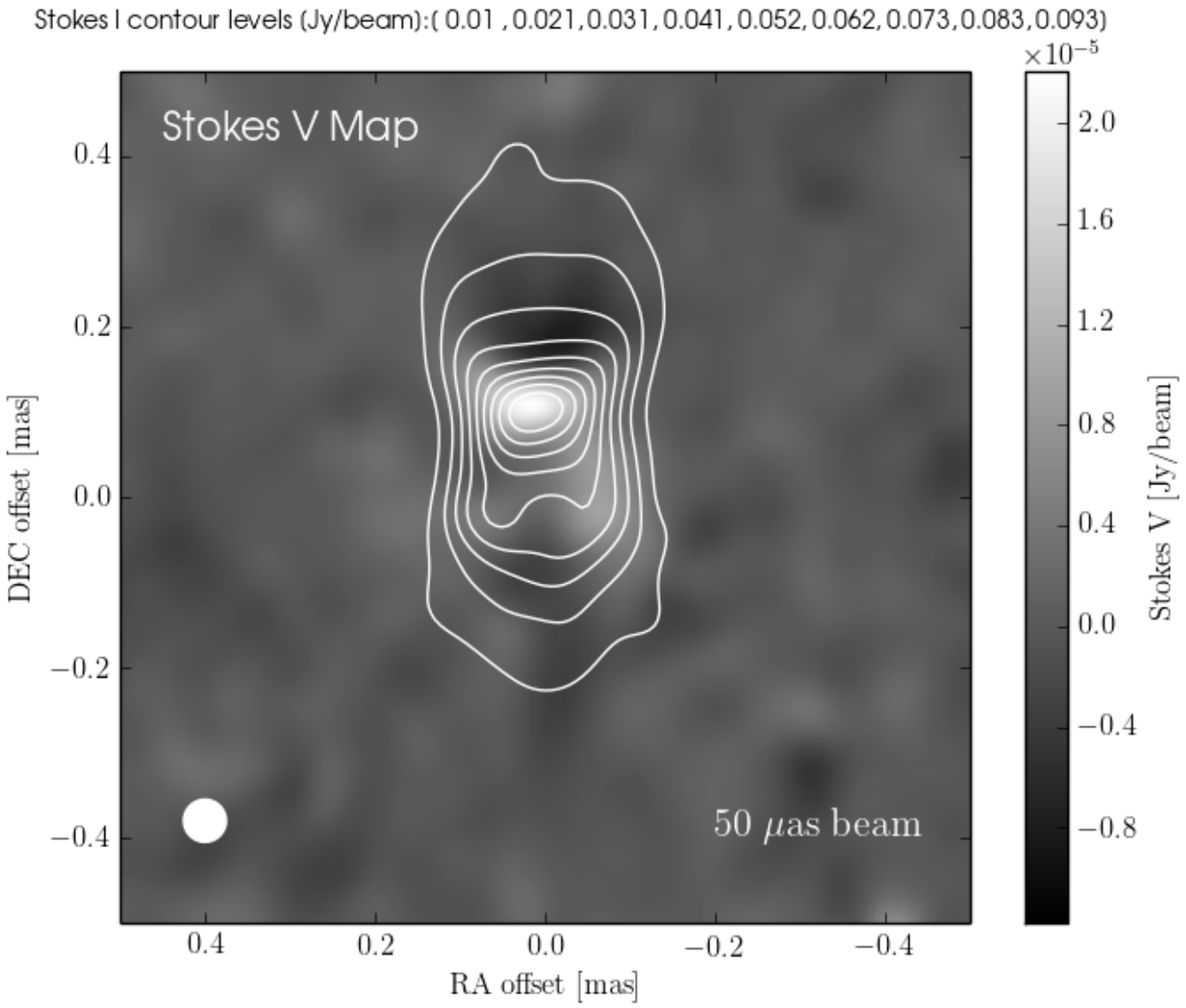

MacDonald (in prep)

RMHD Imaging

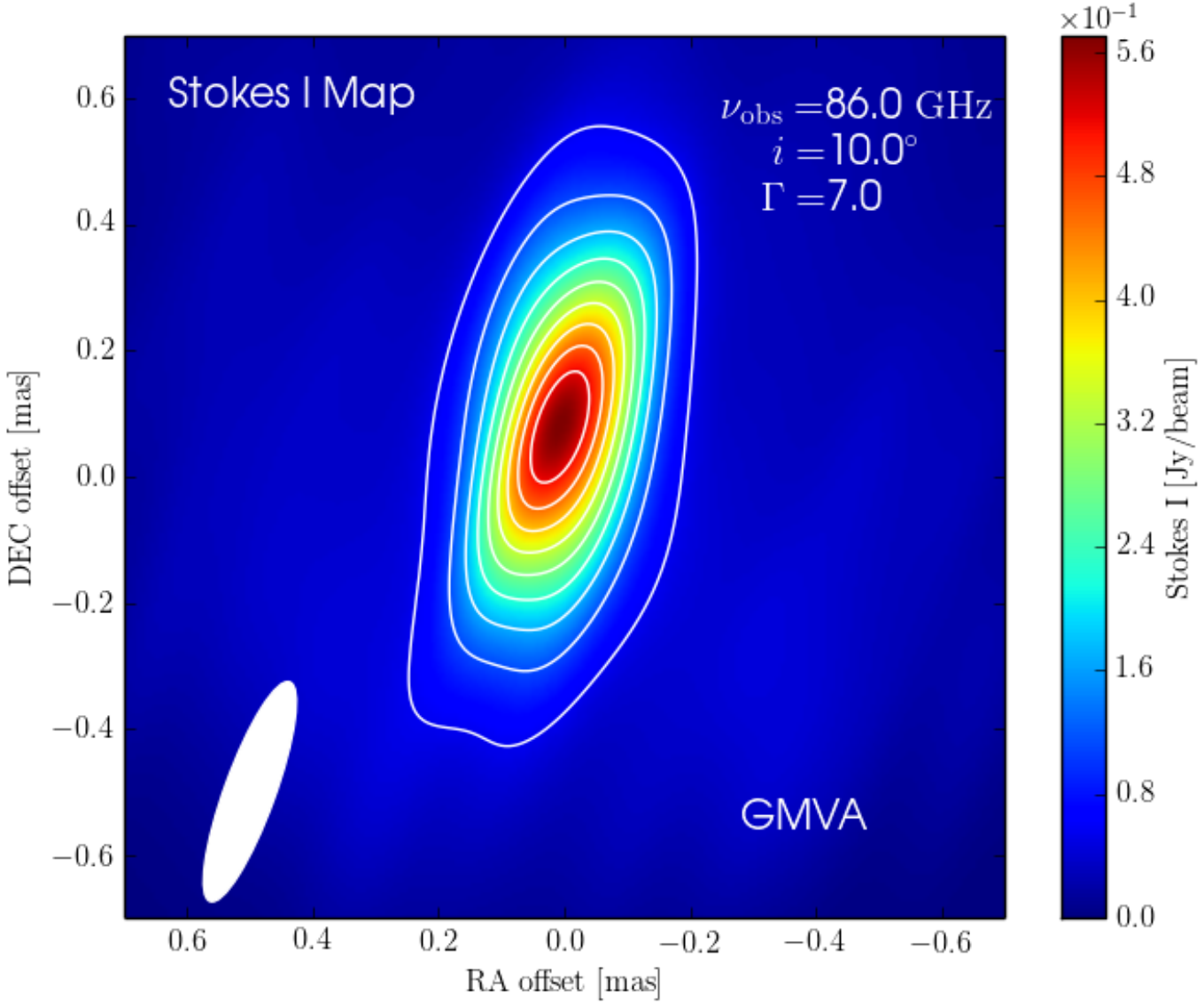

MacDonald (in prep)

Stacked Rotation Measure Mapping

MOJAVE Program

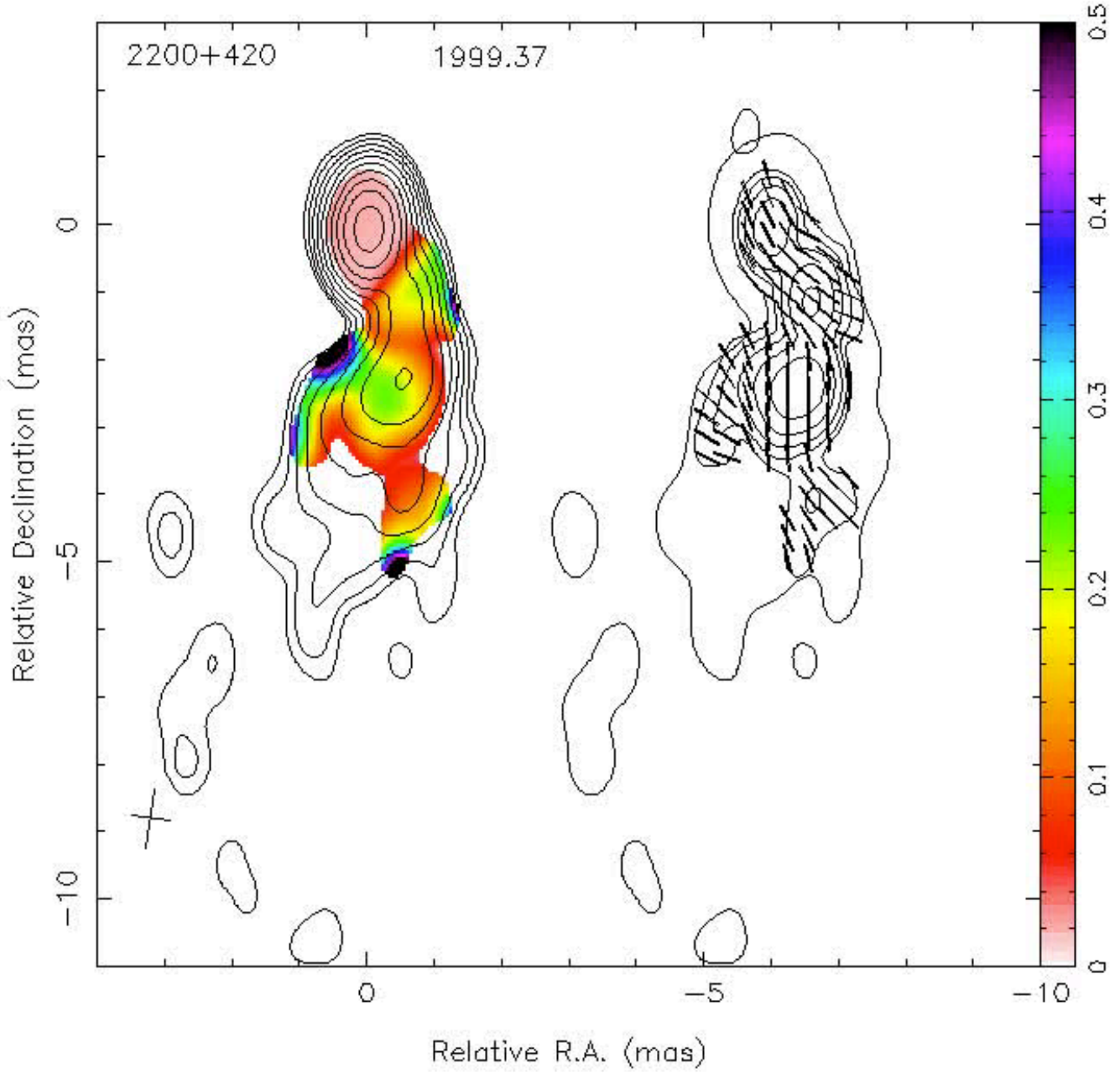

Lister et al. (2017)

Boston University Blazar Group

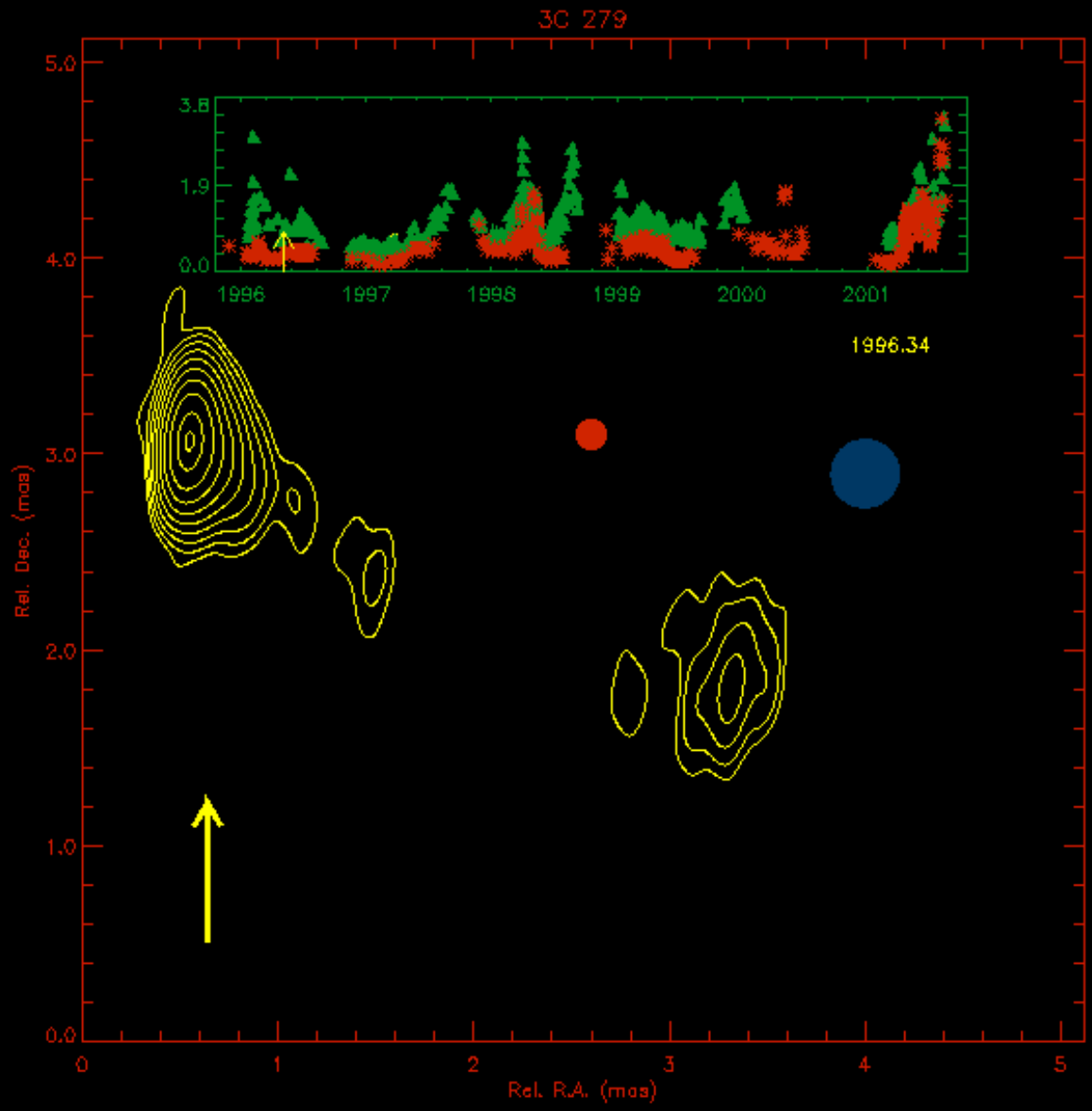

Jorstad et al. (2017)

RMHD Modeling

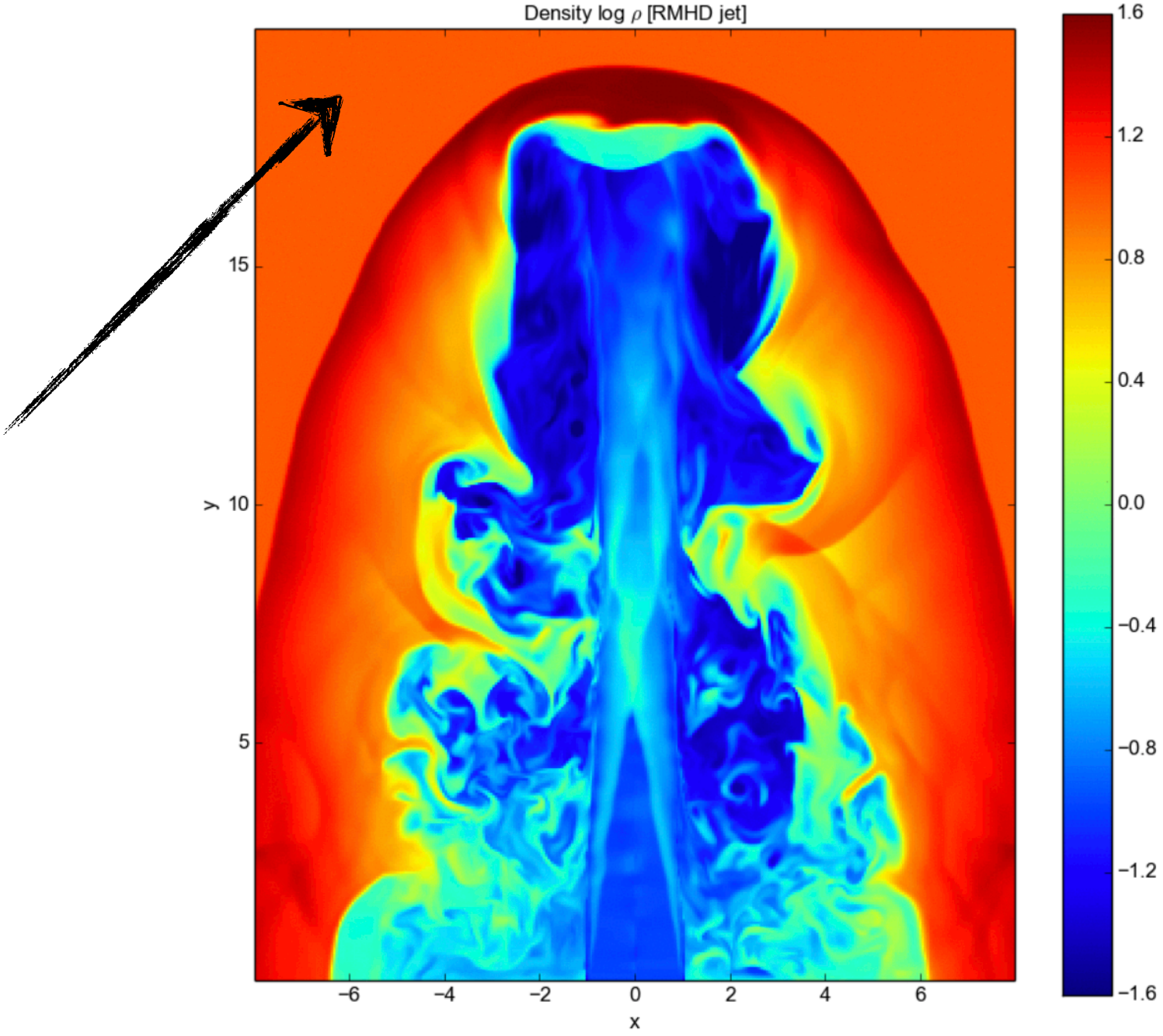

Radio Map Stacking

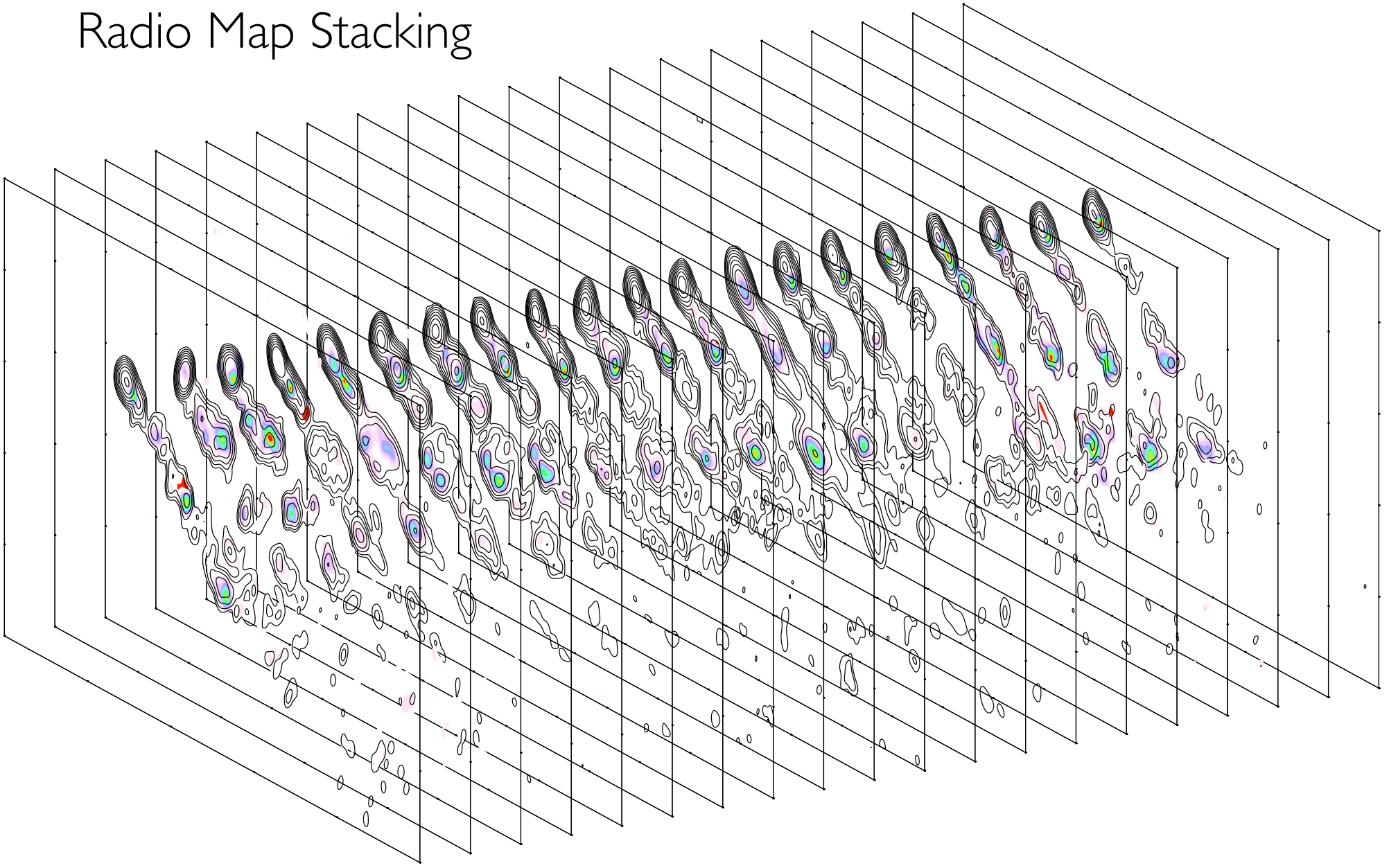

MacDonald, Jorstad, & Marscher (2017)

Mon. Not. R. Astron. Soc. **386,** 619–626 (2008) doi:10.1111/j.1365-2966.2008.13087.x

Aligning VLBI images of active galactic nuclei at different frequencies

S. M. Croke[1,2] and D. C. Gabuzda[3]★

[1]*Department of Physics, University of Strathclyde, Glasgow G4 0NG*
[2]*Department of Mathematics, University of Glasgow, Glasgow G12 8QW*
[3]*Department of Physics, University College Cork, Cork, Ireland*

Accepted 2008 February 6. Received 2008 January 10; in original form 2007 September 8

ABSTRACT

Many important techniques for investigating the properties of extragalactic radio sources, such as spectral-index and rotation-measure mapping, involve the comparison of images at two or more frequencies. In the case of radio interferometric data, this can be done by comparing the CLEAN maps obtained at the different frequencies. However, intrinsic differences in images due to the frequency dependence of the radio emission can be distorted by additional differences that arise due to source variability (if the data to be compared are obtained at different times), image misalignment, and the frequency dependence of the sensitivity to weak emission and the angular resolution provided by the observations (the resolution of an interferometer depends on the lengths of its baselines in units of the observing wavelength). These effects must be corrected for as best as possible before multifrequency data comparison techniques can be applied. We consider the origins for the aforementioned factors, outline the standard techniques used to overcome these difficulties, and describe in detail a technique developed by us, based on the cross-correlation technique widely used in other fields, to correct for misalignments between maps at different frequencies.

Key words: techniques: image processing – galaxies: active.

Croke & Gabuzda (2008)

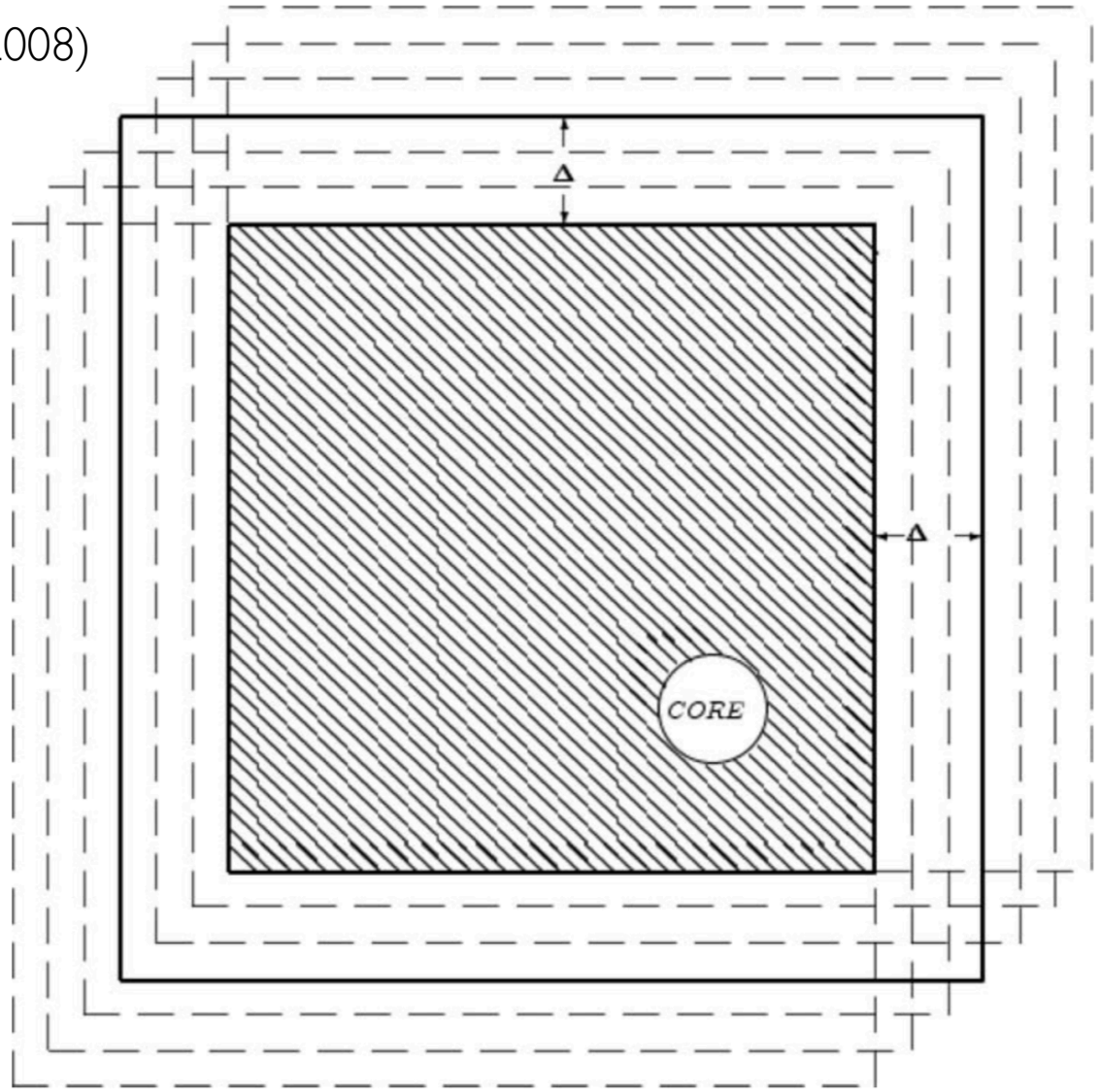

Figure 1. Implementation of image alignment by cross-correlation. A subarea (shaded region) of the first map (outlined in bold) is compared with the overlying region of the second map. This subarea remains constant, while the corresponding region of the second map changes as it is shifted relative to the first map (some possible shifted positions are outlined with dashed lines). The cross-correlation coefficient between the two regions, given by equation (1), is computed each time to provide a measure of how well the areas are correlated. The method assumes that the highest correlation is achieved when the areas being compared refer to the same physical region of the sky. The circle labelled 'core' represents a region with a specified elliptical or circular shape (corresponding to the beam shape) coincident with the position of the optically thick core, which is omitted from Map 1 during the cross-correlation calculations.

Croke & Gabuzda (2008)

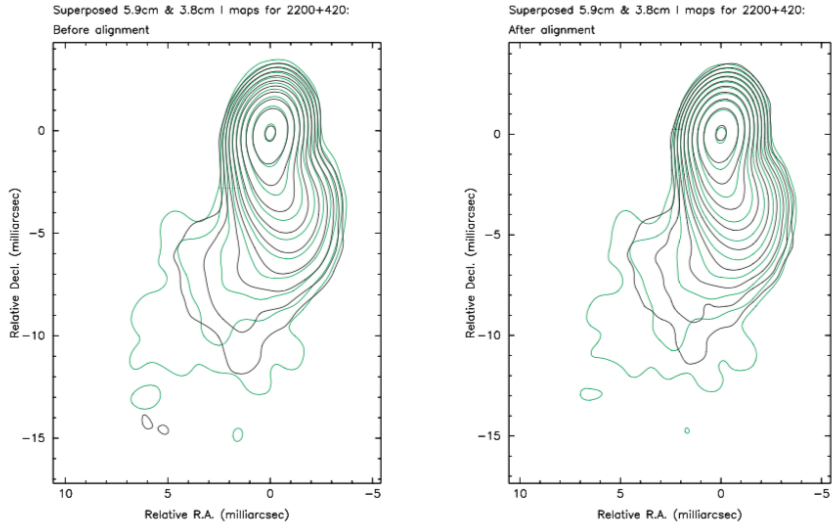

Figure 4. Maps of 2200+420 before (left-hand panel) and after (right-hand panel) alignment, showing I contours at 5.1 GHz in green, with I contours at 7.9 GHz superposed in black. The convolving beam was 2.25×1.59 mas^2 in position angle $-13\overset{\circ}{.}8$, and was the same in all cases. The bottom contour levels are ± 0.20, and the contours increase in steps of 1.98. The peak brightness values are 1940 mJy beam^{-1} (7.9 GHz) and 1520 mJy beam^{-1} (5.1 GHz). In this case, there is no compact, distinct optically thin feature on which to base the derived shift between the two images, but the algorithm has nevertheless properly aligned the images, as is clear from a comparison of the corresponding spectral-index maps in Fig. 5.

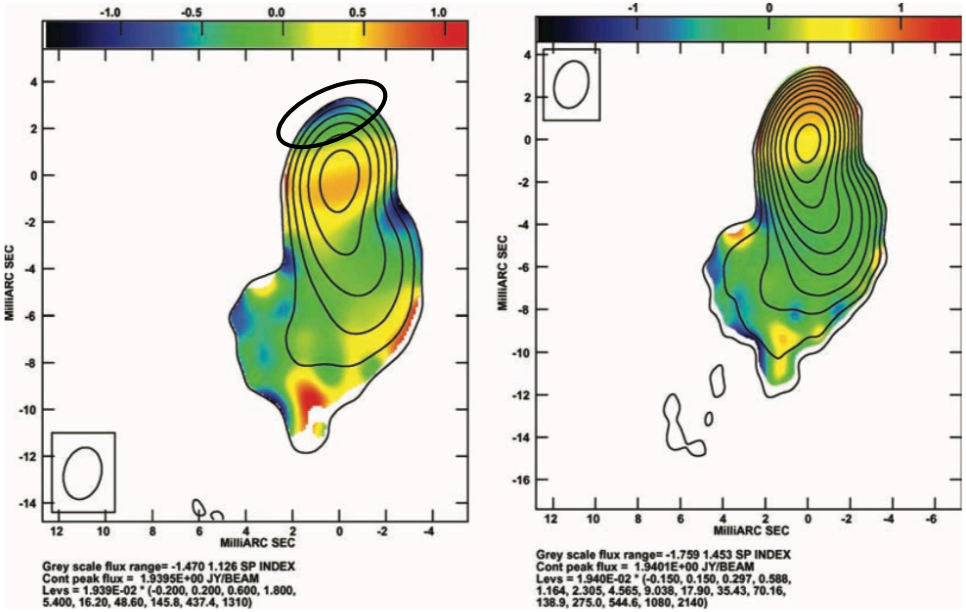

Figure 5. Spectral-index maps of 2200+420 before (left-hand panel) and after (right-hand panel) alignment, with the contours of total intensity at 7.9 GHz from Fig. 4 superposed. The convolving beam is shown in an upper corner of each image. The shown ranges of spectral indices are from -1.47 to 1.13 (left-hand panel) and from -1.76 to $+1.45$ (right-hand panel). False optically thin emission is visible to the north of the I peak in the top spectral-image map. This artefact is absent from the bottom spectral-index map, and the range of spectral indices in the VLBI jet is more moderate.

MOJAVE

Contour Levels (Jy/beam):(0.008, 0.009, 0.012, 0.024, 0.047, 0.094, 0.189, 0.377, 0.754)

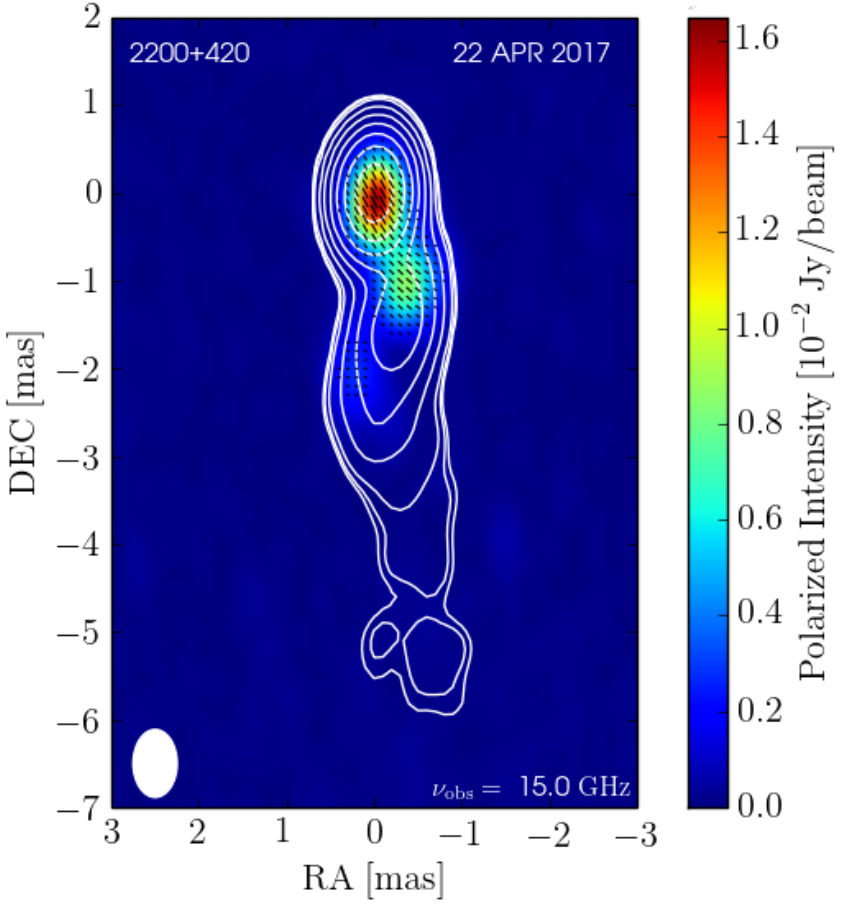

BU

Contour Levels (Jy/beam):(0.001, 0.003, 0.006, 0.011, 0.023, 0.046, 0.091, 0.182, 0.365)

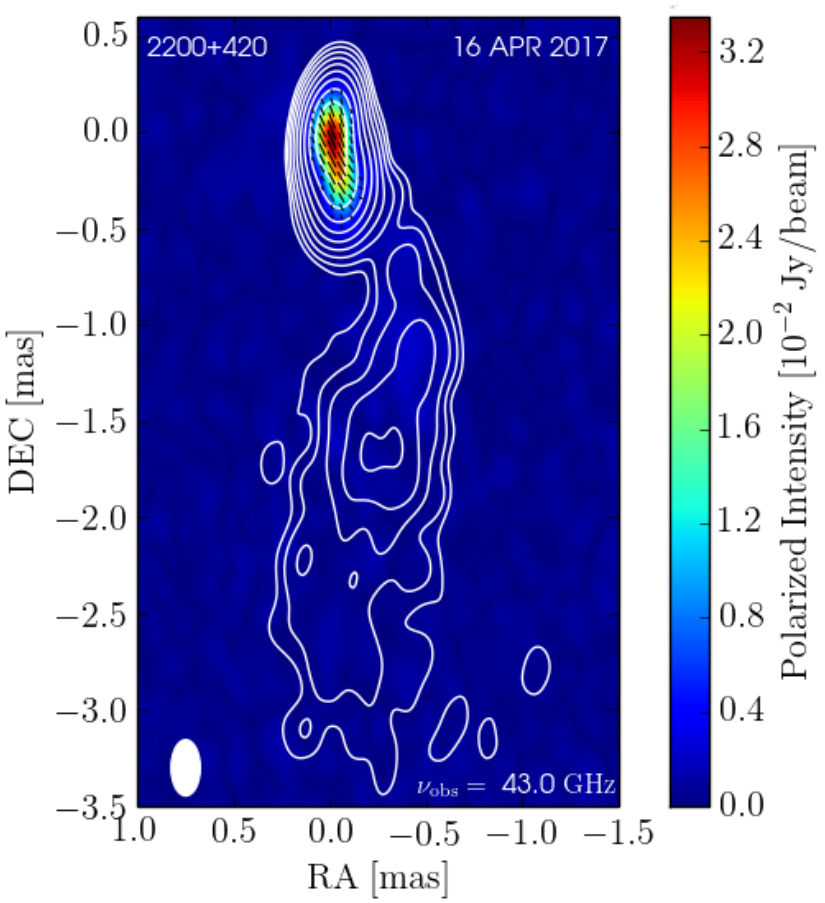

MOJAVE

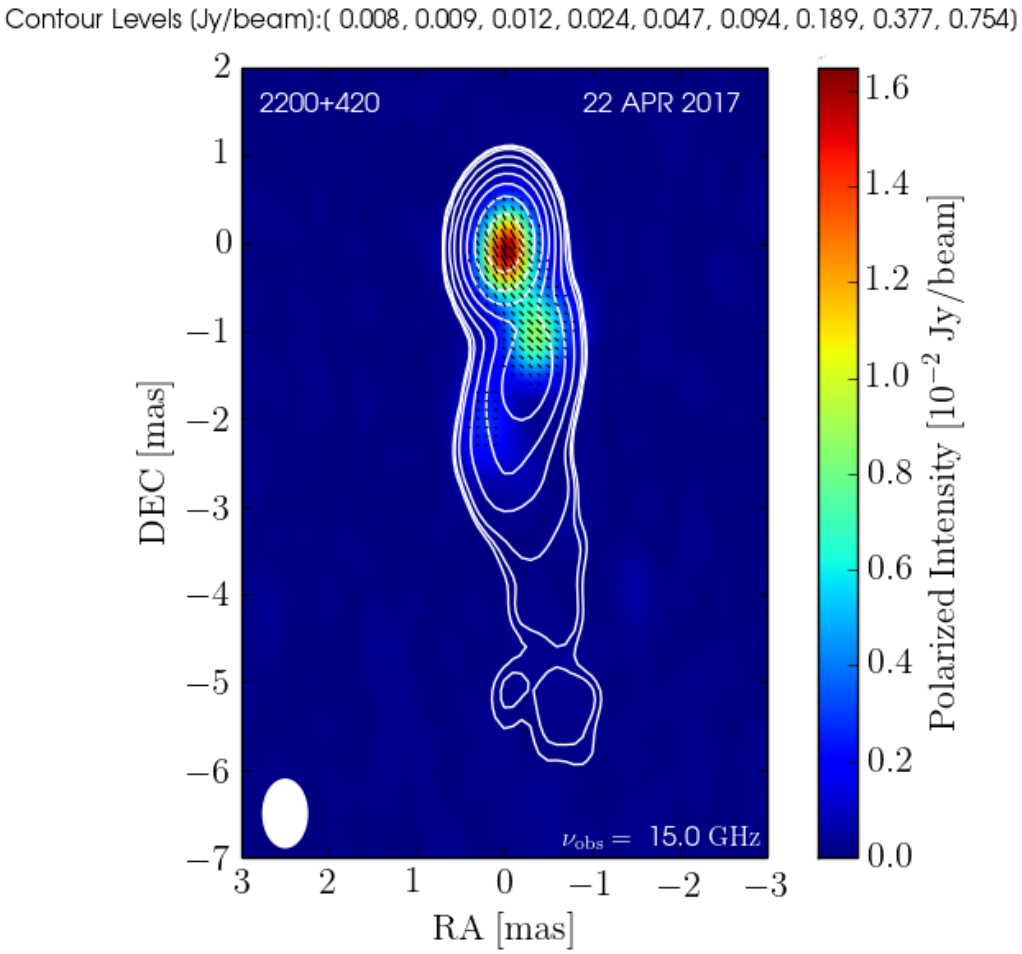
Contour Levels (Jy/beam):(0.008, 0.009, 0.012, 0.024, 0.047, 0.094, 0.189, 0.377, 0.754)
2200+420
22 APR 2017
$\nu_{\rm obs}$ = 15.0 GHz
DEC [mas]
RA [mas]
Polarized Intensity [10^{-2} Jy/beam]

BU

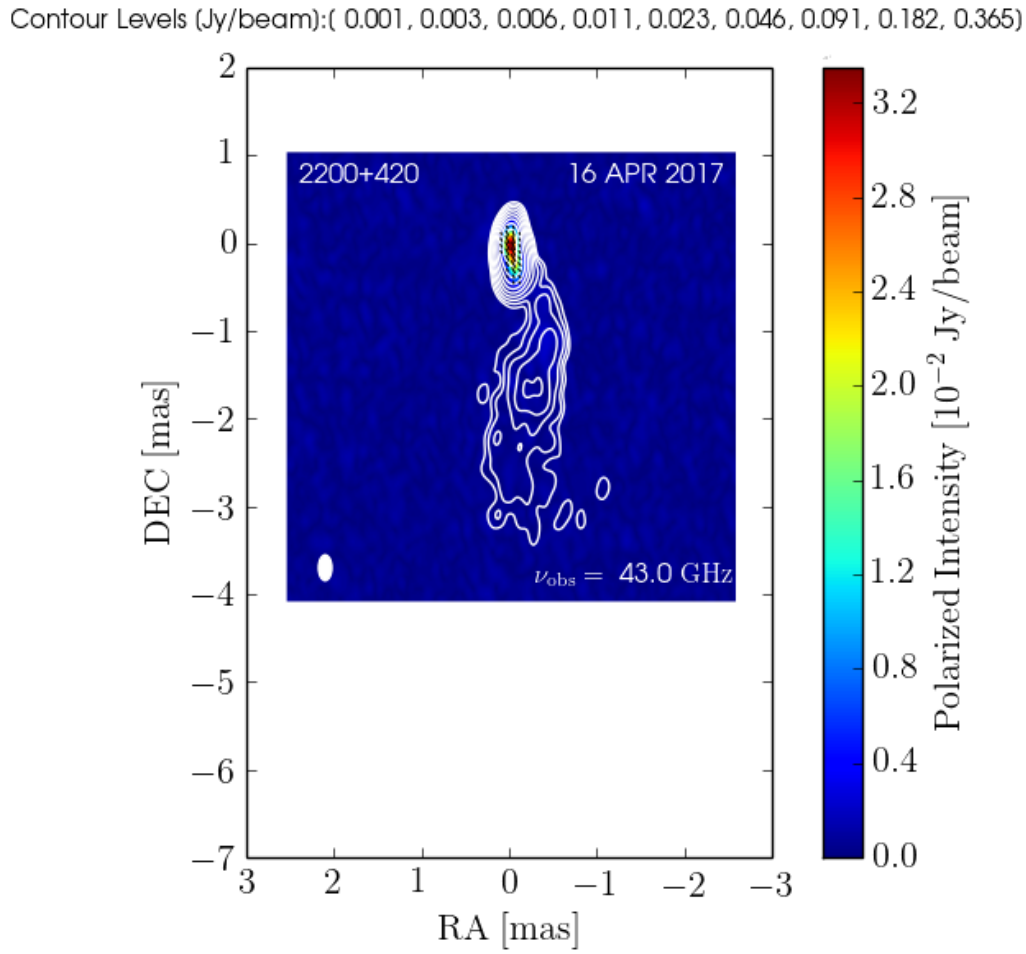
Contour Levels (Jy/beam):(0.001, 0.003, 0.006, 0.011, 0.023, 0.046, 0.091, 0.182, 0.365)
2200+420
16 APR 2017
$\nu_{\rm obs}$ = 43.0 GHz
DEC [mas]
RA [mas]
Polarized Intensity [10^{-2} Jy/beam]

MOJAVE

BU

Contour Levels (Jy/beam):(0.008, 0.009, 0.012, 0.024, 0.047, 0.094, 0.189, 0.377, 0.754)

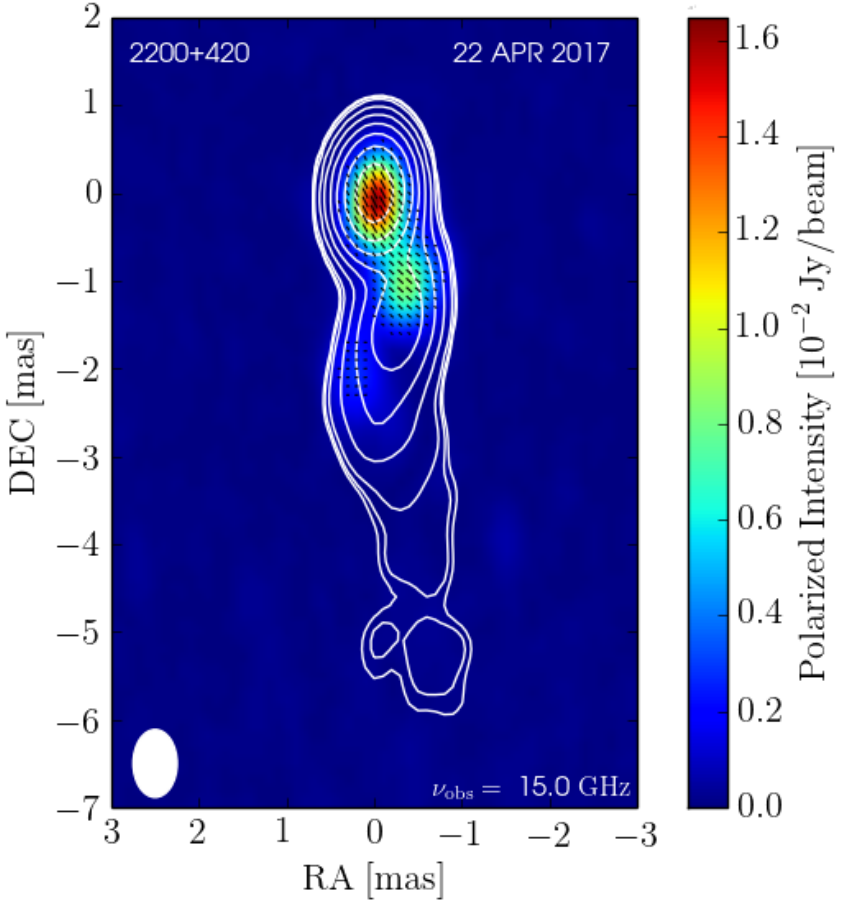

+

Contour Levels (Jy/beam):(0.007, 0.008, 0.011, 0.021, 0.043, 0.085, 0.171, 0.342, 0.684)

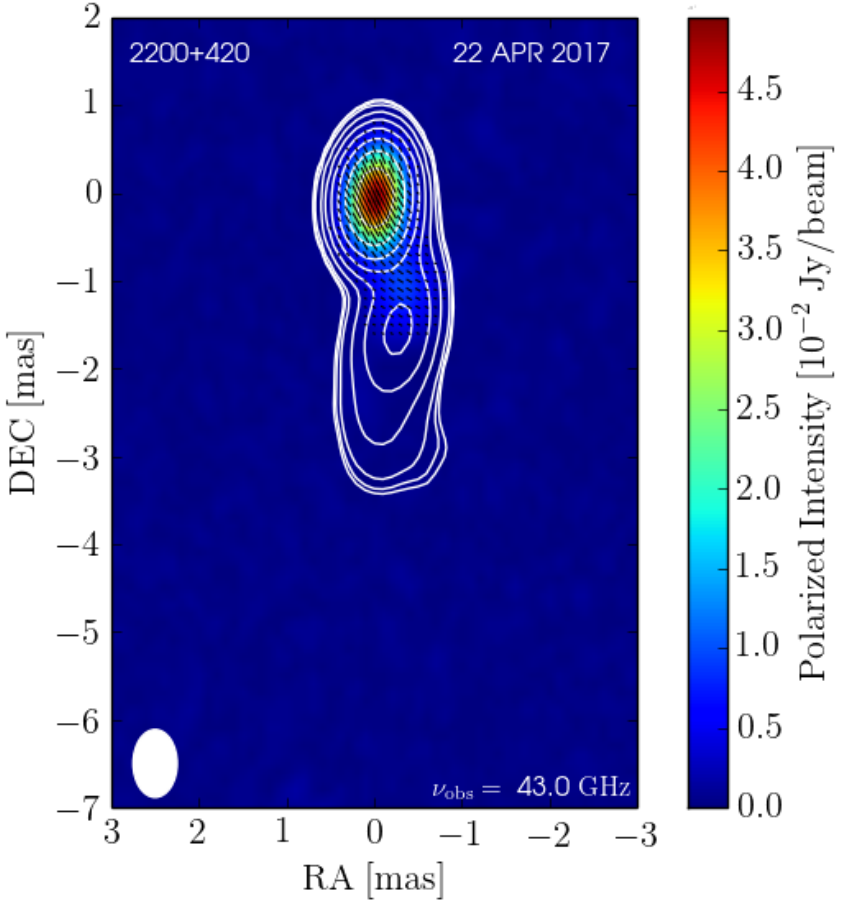

Contour Levels (Jy/beam):(0.007, 0.008, 0.011, 0.021, 0.043, 0.085, 0.171, 0.342, 0.684)

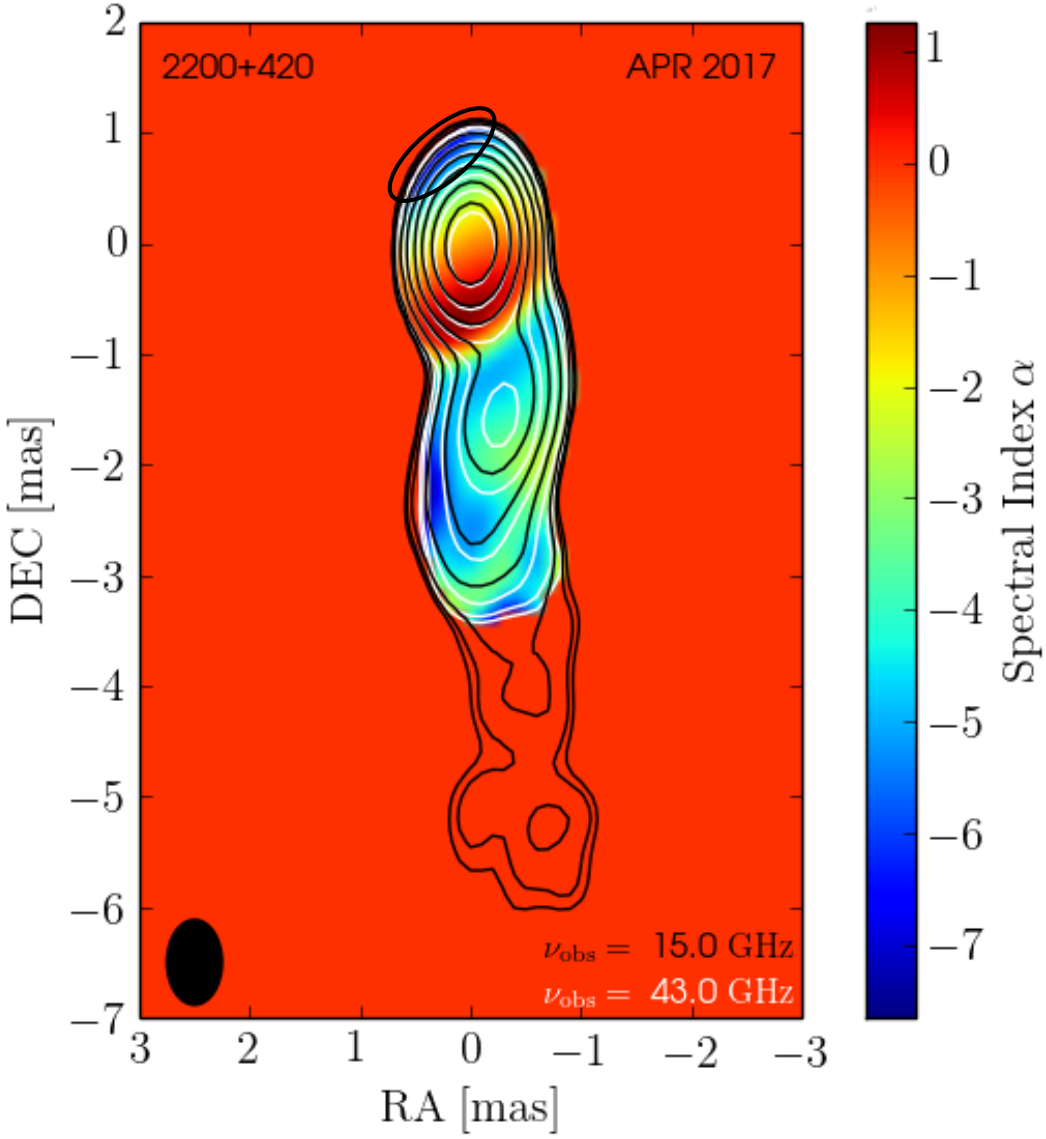

$$\alpha = \frac{\log\left(\frac{I_{\nu_1}}{I_{\nu_2}}\right)}{\log\left(\frac{\nu_1}{\nu_2}\right)}$$

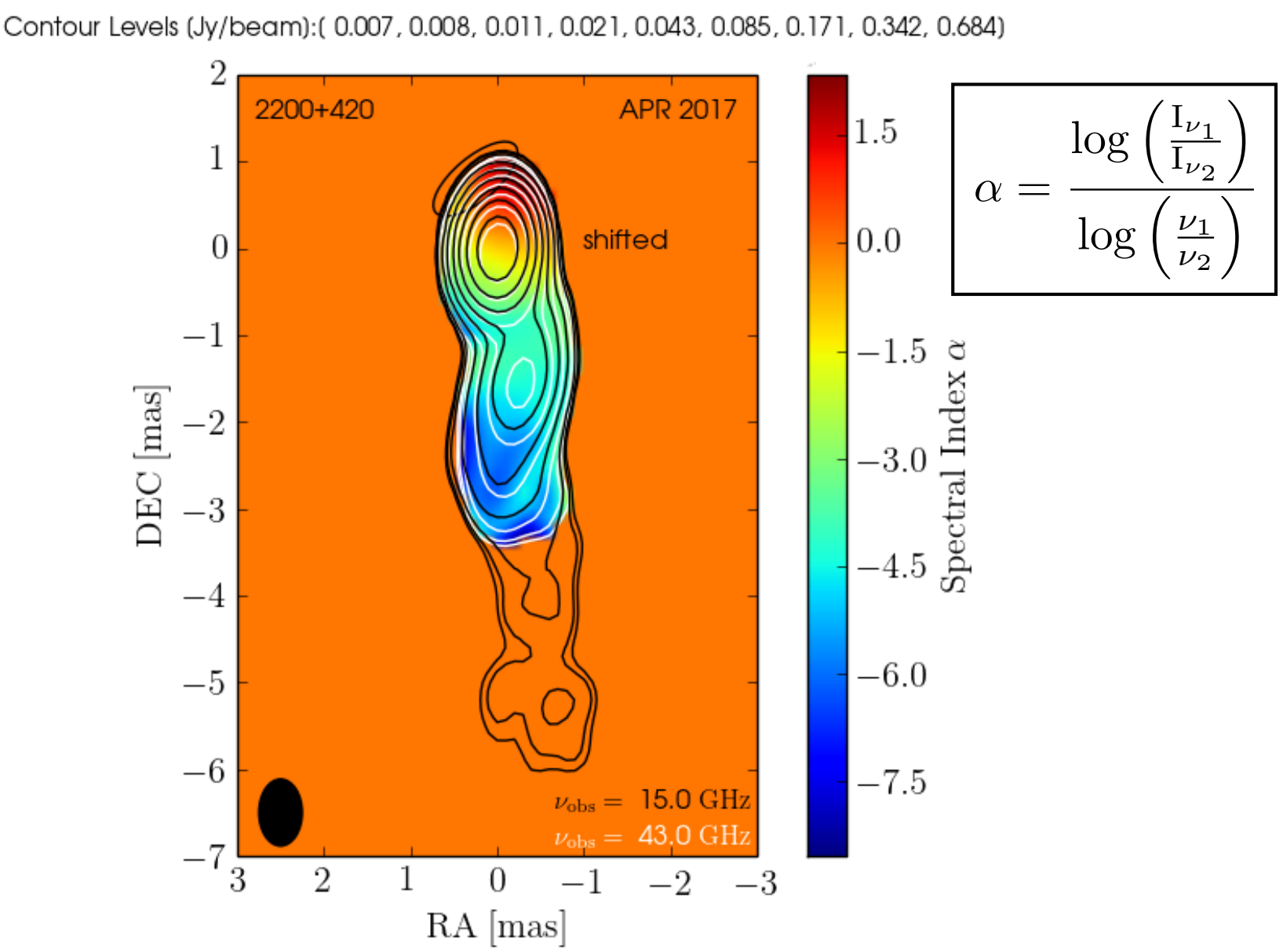
Contour Levels (Jy/beam):(0.007, 0.008, 0.011, 0.021, 0.043, 0.085, 0.171, 0.342, 0.684)
2200+420
APR 2017
shifted
$\nu_{\rm obs} =$ 15.0 GHz
$\nu_{\rm obs} =$ 43.0 GHz
DEC [mas]
RA [mas]
Spectral Index α
$\alpha = \frac{\log\left(\frac{I_{\nu_1}}{I_{\nu_2}}\right)}{\log\left(\frac{\nu_1}{\nu_2}\right)}$

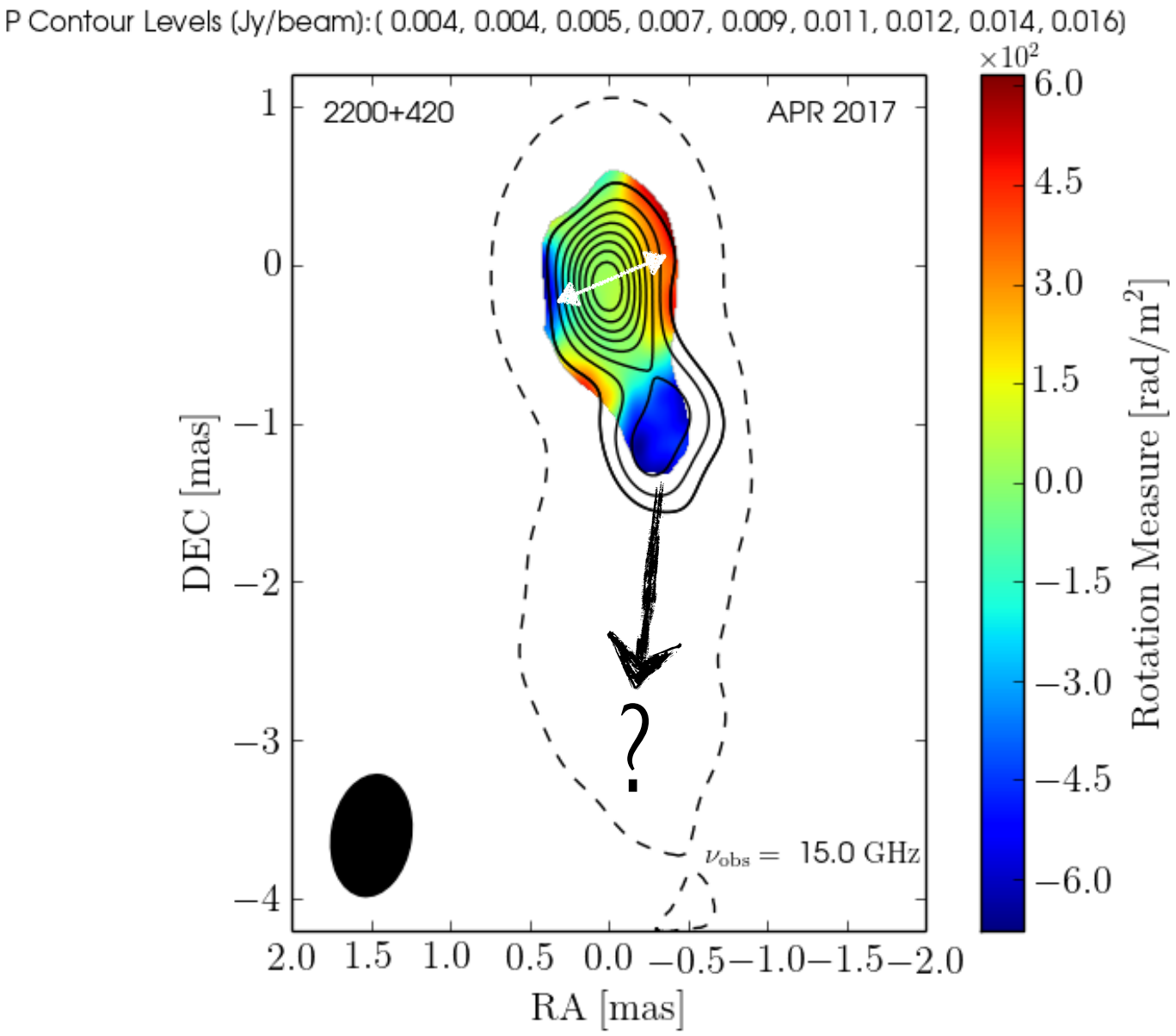
P Contour Levels (Jy/beam):(0.004, 0.004, 0.005, 0.007, 0.009, 0.011, 0.012, 0.014, 0.016)
2200+420
APR 2017
$\nu_{\rm obs}$ = 15.0 GHz
?
DEC [mas]
RA [mas]
$\times 10^2$
Rotation Measure [rad/m^2]


Questions?

TEMZ Imaging

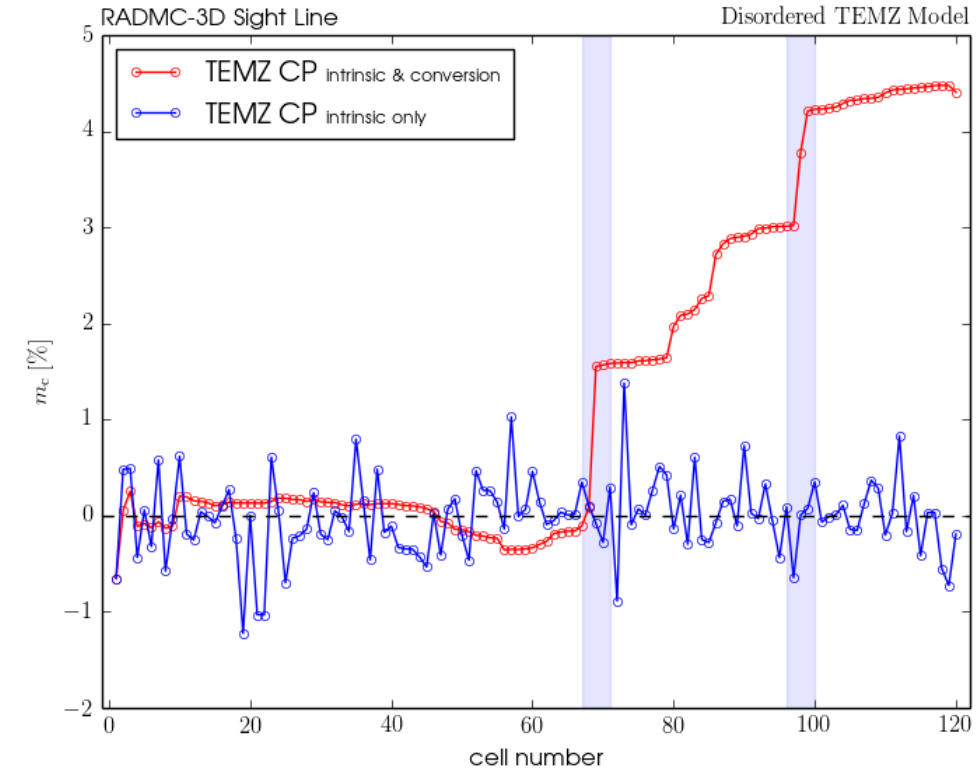

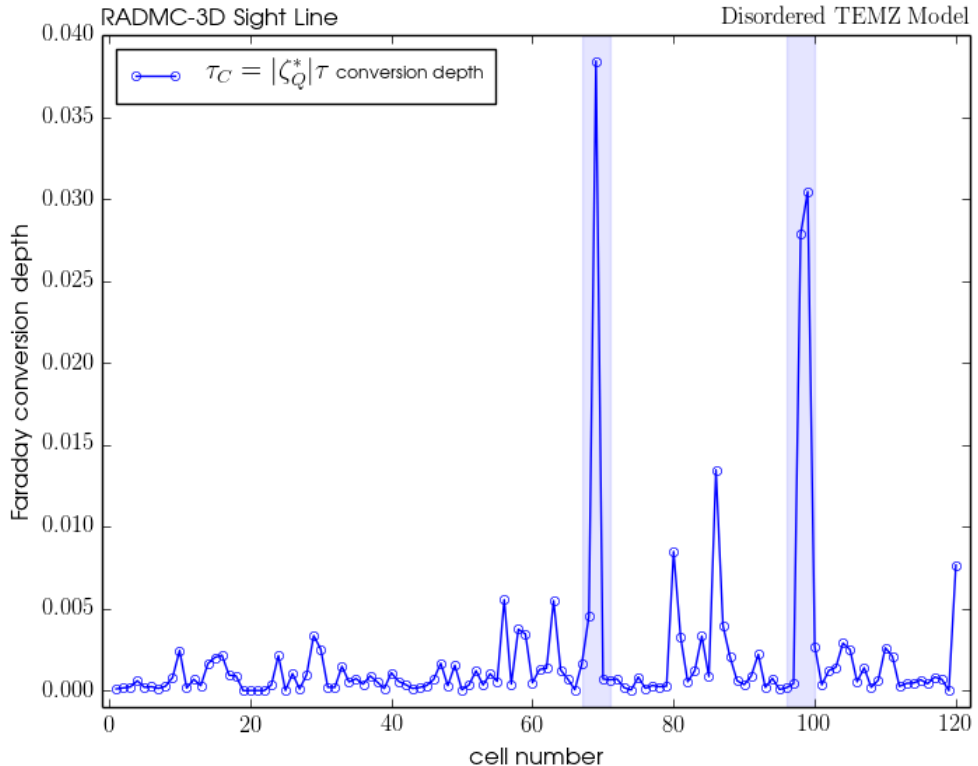

MacDonald & Marscher
(in press)